Magnetic survey forward modelling and paleomagnetic reconstruction of the South China Block in the Ediacaran

by

Benjamin Lysak

A thesis submitted in partial fulfillment of the requirements for the degree of

Master of Science
in
Geophysics

Department of Physics
University of Alberta

Abstract

Studying the Earth's magnetic field and Earth materials response to the magnetic field provides us with a plethora of information of underground features, paleoclimatology, and paleogeographic features. Measuring magnetic intensity is one of the fastest geophysical survey methods used in research and natural resource exploration. Accurate modeling of two-dimensional magnetic anomalies is crucial in resource estimation and exploration plans. Paleomagnetism is the study of Earth's ancient magnetic field that is recorded in rocks. By determining the primary magnetization stored in a rock along with its age we can compute paleomagnetic poles which in turn give us information about the latitude of where it was deposited and tectonic block rotation, using this information is the only latitudinal constraint that can be used in paleogeographic reconstructions.

The very first computational algorithm and most referred in literature is that of Talwani and Heirtzler (1964) for calculating of the magnetic anomaly caused by two-dimensional irregular shape subsurface structure has particular fundamental and educational significance in geophysics theory. We re-derive this algorithm from first principles and discuss previous derivation omissions. Our resulting solution differs from the original publication. Based on our new solution we present the two-dimensional forward magnetic modeling software and associated tutorials which are available for download from the website www.ualberta.ca/~vadim/software.htm. Additionally, we include the computation of the remnant magnetization which can be found using already published apparent polar wonder paths.

The paleogeography of the South China Block (SCB) from the breakup of Rodinia to the assemblage of Pangea is widely debated and many alternative models have been produced due to the lack of reliable paleomagnetic poles before the Late Paleozoic. Published Ediacaran poles do not match each other are unreliable based on criteria outlines in Van der Voo (1990) and do not determine primary magnetization. We present a new study from the boundary of Doushantuo and Dengying Formations (551 Ma) of the SCB that passed both polarity and fold tests. We have primary directions at the top of the Doshantuo formation and bottom of the Dengying formation from four sections that are separated by 10 - 120 km located in the South of the Shaanxi Province, China. From these four sampled sections two sections showed results with primary magnetizations. We obtained both low and high temperature components performing thermal demagnetization. The high temperature component can be evaluated from both component directions and demagnetization circles in both normal and reverse polarities. The low temperature component directions are usually scattered with some clustering close to the present field of the Earth. The new paleogeographic position of the SCB is at the equator which differs from many publications. Using our new pole, we re-evaluate the Ediacaran paleogeography of the South China Block and its relationship with Gondwana continents.

Preface

Chapter 2 of this thesis has been published as Kravchinsky, V. A., Hnatyshin, D., Lysak, B., & Alemie, W. (2019). Computation of magnetic anomalies caused by two dimensional structures of arbitrary shape: derivation and Matlab implementation. *Geophysical Research Letters*, https://doi.org/10.1029/2019GL082767. I was responsible for rederiving the original algorithm of Talwani and Heirtzler (1964) as well as the comparison to different magnetic modelling codes and the conclusion. V.A.K., the primary author, conceived the study, wrote the first version of the software, derived the new algorithm with W.A., wrote the first draft of the manuscript with D.H. D.H. wrote the GUI. V.A.K., D.H. and B.L. contributed to the writing of different parts of the consequent versions of the manuscript.

Chapter 3 of this thesis forms part of an international collaboration led by V.A. Kravchinsky from the University of Alberta, corresponding with Mathew Domeier from the University of Oslo, Norway, Xingliang Zhang and Rui Zhang from the Northwest University, Xi'an China. Together with lab technician L. Koukhar we completed laboratory measurements, and I performed analysis and interpretation with guidance from Vadim Kravchinsky and Mathew Domeier. The field work and preliminary work for this project was completed by Vadim Kravchinsky, Mathew Domeier, Xingliang Zhang and Rui Zhang.

Acknowledgements

I would like to express my gratitude and thank my loving family for the constant support throughout my graduate studies. Your positive encouragement is the reason this thesis could be completed. V. A. Kravchinsky, my supervisor, was outstanding in his wisdom, guidance, teaching and mentorship. Your encouragement, friendliness, and sense of humor made working with you easy and an absolute pleasure. Thank you L. Koukhar for your help in the lab with cutting, measuring, organizing samples, and delicious treats. You were an invaluable asset for me to complete this thesis. M. Domeier for your teaching and guidance in Norway and throughout my Ediacaran project. Petter Silkoset for your guidance in the Ivear Greavor Geomagnetic Laboratory. My thesis committee members Dr. M. Unsworth, S. Johnston and Y. J. Gu for their comments and feedback for improvement on this thesis. Ryan Borowiecki and Katya Kozmina, I will always remember our discussions about work and life. You were both wonderful encouragement and easy to work with throughout my studies. Lastly, a thank you to all the friends, wonderful teachers and mentors I have acquired throughout my graduate studies. This chapter of my life has shaped me to be who I am today, and I will always be grateful for all of you.

Table of Contents

List of Tables

List of Figures

Abbreviations

APWP – Apparent Polar Wander Path

HTC – High Temperature Component

LC – Low Temperature or Coercivity Component

NCB - North China Block

PCA – Principal Component Analysis

SWE – Shuram Wonoka Excursion

SCB – South China Block

Chapter 1: Introduction

The Earth's magnetic field shields us from dangerous solar radiation, allows us to navigate the Earth, find ore bodies in the ground and reconstruct how Earth's continents have moved. In geophysical prospecting one of the most commonly used methods is measurement of the total intensity of the magnetic field. This is used as data collection and processing can be done quickly, and the anomaly contrasts are easily observable. In paleogeographic reconstructions measurement of primary remnant magnetization provide the only means of determining paleolatitude of plates.

The response of a magnetic mineral to an applied field is defined as magnetic susceptibility. There are three major magnetic susceptibility responses to the applied field; diamagnetic, paramagnetic, and ferromagnetic. A diamagnetic material responds in the opposite direction of the applied magnetic field. Paramagnetic and ferromagnetic materials respond producing a magnetic field in the same direction of the applied field the difference being that ferromagnetic materials maintain the field direction even after the field is removed.

Magnetic anomalies are caused by the interaction of Earth's magnetic field with magnetic minerals. The two properties that make up the magnetic anomaly are the magnetic susceptibility and remnant magnetization. Remnant magnetization is the magnetic field of the mineral that was acquired either during deposition or metamorphism occurring since deposition and is

permanently stored in the rock. The super position of the two are what creates the magnetic anomaly. Mapping of the Earth's magnetic field can be done in several ways.

- Measuring the total intensity of the Earth's magnetic field
- Measuring the vector components of the Earth's magnetic field
- Measuring the gradient (vertical or horizontal) of the Earth's magnetic field

There exist two geophysical problems, the forward problem or the inverse problem, to interpret and model the magnetic survey data. The forward problem in geophysics is designed to predict the data response to the subsurface geological model. The inverse problem in geophysics requires an approximation based on mathematical models and constraints in order to reconstruct the subsurface geological features. Depending on the amount of geologic and geophysical information available determines which method or combination of methods are chosen to solve the data.

The very first and most cited among forward magnetic modelling computational algorithm was developed by Talwani and Heirtzler (1962). Upon implementation for use with new software, written in high-level programing language Matlab, this algorithm produced errors due to definition of trigonometric functions. This created the questions of what the correct algorithm is to use for computational forward modelling and what are the issues with the previous algorithm derived by Talwani and Heirtzler (1964). The results of this investigation are explained and highlighted in chapter 2 of this thesis. The results of chapter 2 have been published in Geophysical Research Letters (https://doi.org/10.1029/2019GL082767).

Chapter 3 deals with paleogeographic reconstruction of continental positions due to continental drift. Paleogeographic reconstructions are usually based on paleontology, sedimentary similarities, tectonic markers, and paleomagnetic studies. The Ediacaran is arguably one of the most important periods in the evolution of life (Fike et al., 2006; Grotzing et al., 2011; Williams and Schmidt, 2018). It was during this time that the oceans became increasingly oxygenated creating an environment that was favorable for larger multicellular life (Fike et al., 2006). Paleogeographic reconstructions play crucial role in many paleoclimate systems, influencing ocean and atmospheric circulation which affects ocean chemistry (Williams and Schmidt, 2018).

During the Ediacaran there was the final amalgamation of the supercontinent Gondwana which is widely agreed upon as consisting of present-day Australia, India, Oman, South America, Africa, and East Antarctica (Figure 1.1) (Veevers, 2004; Cawood et al., 2018; Li et al., 2018; Torsvik and Cocks 2013). Major continents not accounted for as being part of Gondwana are Laurentia, Baltica, and Siberia (Torsvik and Cocks, 2013). Often not included in reconstructions are the North China Block (NCB) and the South China Block (SCB) due to the lack of reliable paleomagnetic data. The SCB is of particular interest as it contains many well-preserved biota and geochemical signatures, though due to lack of paleomagnetic data has been modelled in a plethora of different locations in the global paleogeographic maps (Li et al., 2018). Chapter 3 of this thesis reviews our study on rocks that span in age from the beginning of the Ediacaran to the early Cambrian from the SCB. The results of this study provide the first reliable paleomagnetic

pole for the SCB dated prior to the Ediacaran-Cambrian transition and provides the first Apparent Polar Wander Path for the South China Block that reliably spans into the Ediacaran.

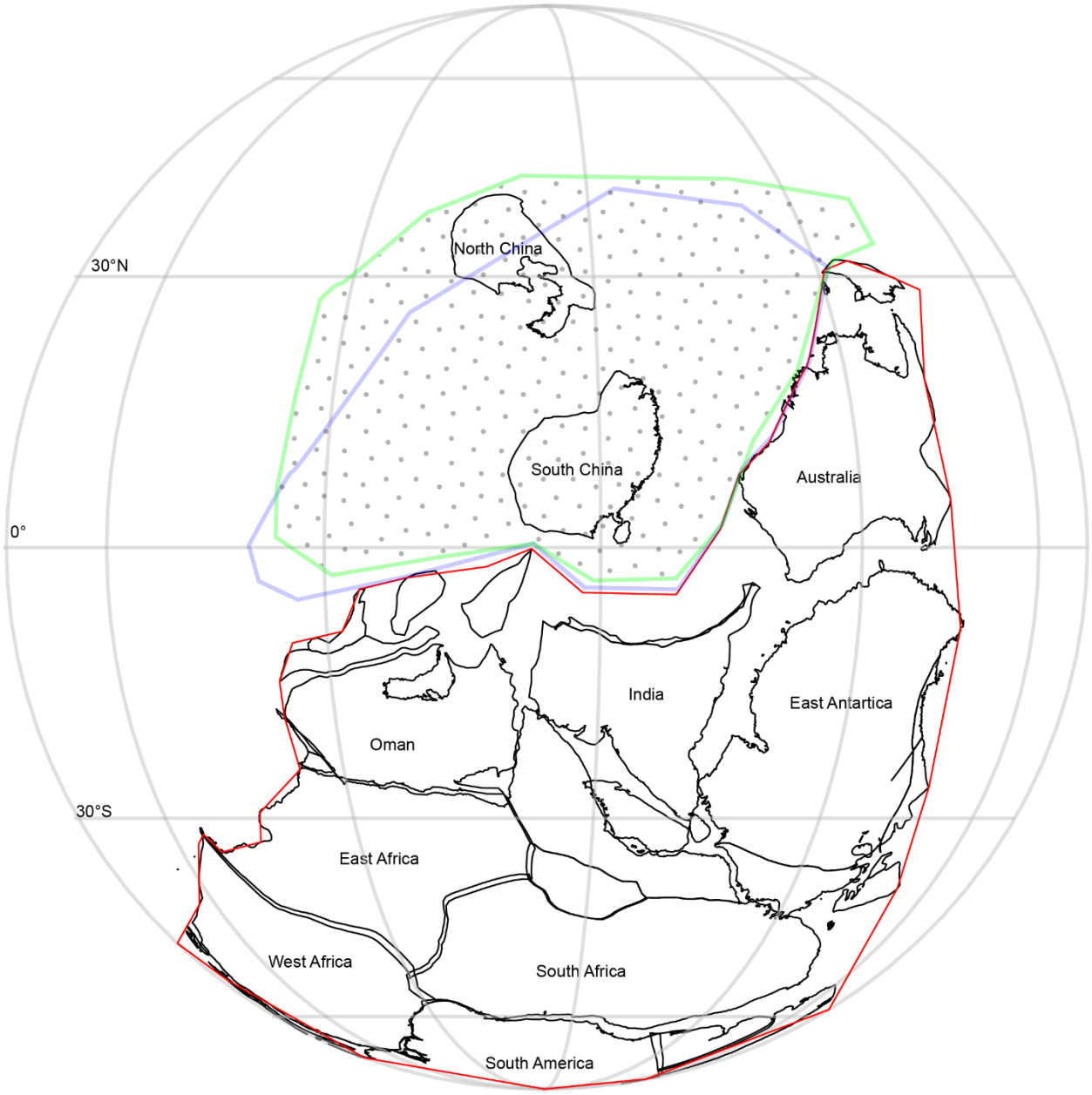

Figure 1.1. North China Block and the South China Block and construction of Gondwana at 540 Ma based on Torsvik and Cocks (2013) reconstruction. Plate contours are from present day coastlines neglecting deformation. The polka dots and green outline represents the range of reconstructions for the North China Block and blue outline represents the range of constructions for the South China Block. Figure was created using the Gplates software (Muller et al., 2018).

Chapter 2: Computation of magnetic anomalies caused by two dimensional structures of arbitrary shape: derivation and Matlab implementation[1]

2.1. Introduction

Talwani and Heirtzler (1964) were first to examine a non-magnetic space containing a uniformly magnetized two-dimensional structure approximated by a polygonal prism and to suggest a numerical and computational technique of the forward modeling. A magnetic anomaly above the magnetized body was calculated by analytical formulae using summation of the anomalies due to semi-infinite prisms limited on one side by a segment of the polygon. The derivation of the mathematical expression for the magnetic anomaly over a two-dimensional body of polygonal cross section was first done in Talwani and Heirtzler (1962). Certainly, it was not the first approach to the problem, a comprehensive review of algorithms and approaches employed prior to 1962 is given in Talwani and Heirtzler (1962). The algorithm was, however, derived specifically for the computation using digital computers and therefore was the first algorithm of such kind.

Since 1964, forward calculations of magnetic anomalies caused by two-dimensional (2-D) and three-dimensional (3-D) bodies have progressed significantly. Talwani (1965) developed a new

[1] A version of this paper has been published as:

Kravchinsky, V. A., Hnatyshin, D., **Lysak, B**., & Alemie, W. (2019). Computation of magnetic anomalies caused by two dimensional structures of arbitrary shape: derivation and Matlab implementation. *Geophysical Research Letters, https://doi.org/10.1029/2019GL082767.*

algorithm to compute the three-dimensional magnetic anomaly for geological bodies of arbitrary shape. Since, both 2- and 3-D forward problems have been developed in various alternative ways. A comprehensive overview of the progress and approaches of the 2-D modeling since 1964 is provided in introductions from Kostrov (2007) and Jeshvaghani and Darijani (2014).

Our initial motivation was to create a Matlab program for educational purposes and for the rapid interpretation of magnetic data. The algorithm of Talwani and Heirtzler (1964) would provide a stable 2-D solution for variety of geological situations. This algorithm is a very effective for magnetic surveys and the publication is the most cited among all existing magnetic forward modeling methods. The first version of our software, however, produced some incorrect anomalies in a number of theoretically modeled situations. Therefore, in this study, we reappraise the derivation that leads us to a different from the Talwani and Heirtzler (1964) solution. Both solutions are compared and discussed below. Further we develop a Matlab p-coded and executable software that has user friendly GUI. The software is a freeware for research and education purposes and can be redistributed among users. Any use of the software should refer to this publication. The software can be downloaded from www.ualberta.ca/vadim/software.htm.

2.2. Important Concepts

Here we introduce the important concepts and notation used for the derivation:

A) Magnetic Susceptibility (χ) - dimensionless. An object's magnetic susceptibility is the constant that indicates how much a material is magnetized in response to the local magnetic field.

B) Magnetization (M) - Units = A/m. Magnetic fields can align the magnetic moments of individual atoms within a material based on that material's magnetic susceptibility. The net magnetic moment of the material per unit volume is magnetization.

C) Induced Magnetization (M_I) is the magnetization associated with the proportion of the material that is aligned with the Earth's magnetic field according to its current inclination and declination.

D) Induced Inclination / Declination. Inclination is the angle the Earth's magnetic field makes with respect with the horizontal. Positive angles are defined as angles that are directed below the horizon. Declination is the difference in angle between true north and horizontal projection of Earth's present day magnetic field. Values increase in the clockwise direction (0^o for North, 90^o for East, etc.).

E) Remnant Magnetization (M_R) is any preserved magnetization not associated with induced magnetization.-Often this is magnetization is associated with the formation of the rock/sediment, or may be associated with recrystalization events (e.g. metamorphism), it is dependent on the direction of the Earth's magnetic field at the time of its acquisition.

F) Remnant Inclination / Declination. Remnant inclination is the angle the source of the remnant magnetization, makes with respect with the horizontal. Positive angles are defined as angles that are directed below the horizon. Remnant declination is the difference in angle between true north and horizontal projection of Earth's ancient magnetic field. Values increase in the clockwise direction (0^o for North, 90^o for East, etc.).

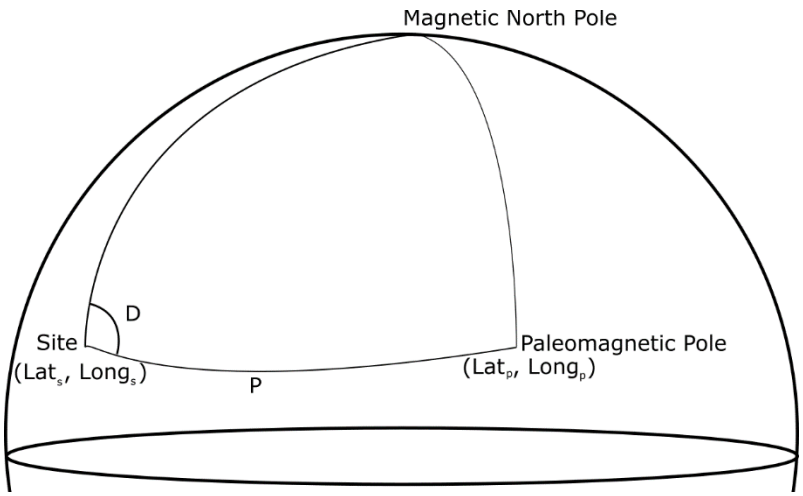

Figure 2.1. Angles from paleomagnetic pole location used for remnant magnetization calculation. D is the declination from the magnetic north pole to the location of the paleomagnetic pole and P is the angular distance between the site and paleomagnetic pole.

The values for remnant inclination and declination vary through time and location but can be estimated if a paleomagnetic pole (paleopole) is known for the object(s) in question. The

paleopole latitude and paleopole longitude can be converted into inclination (I) and declination (D) using MagMod and is based on the following formulas:

$$P = \sin^{-1}\left[\sin(lat_s)\sin\left(lat_p\right) + \cos\left(lat_p\right)\cos\left|long_s - long_p\right|\right] \quad (2.1)$$

$$I = \tan^{-1}[2\tan(P)] \quad (2.2)$$

$$D = \sin^{-1}\left[\sin\left|long_s - long_p\right| * \frac{\cos(lat_p)}{\cos(P)}\right] \quad (2.3)$$

where P = paleolatitude, lat_s is the latitude of the site, lon_s is the longitude of the site, lat_p is the latitude of the paleopole and lon_p is the longitude of the paleopole.

G) Total magnetization of the subsurface structure or small element is a superposition of the induced and remnant magnetizations:

H) A magnetic anomaly is the magnetic field associated with unknown bodies within the subsurface normalized against the local magnetic field (i.e. Earth's magnetic field).

2.3. Calculating Anomalies

Consider that there exists an elemental volume contained within an irregularly shaped body. This elemental volume extends from negative to positive infinity in the y-direction. Bodies of

irregular shapes can be approximated by a polygon, which can be and reduced to solving semi-infinite two-dimensional polygons (Talwani and Heirtzler, 1962). Now consider a small volume element with dimensions dx, dy, dz (Figure 2.1A) located in the geomagnetic field. The total magnetization of the volume is a superposition of both induced and remnant magnetizations which co-exist.

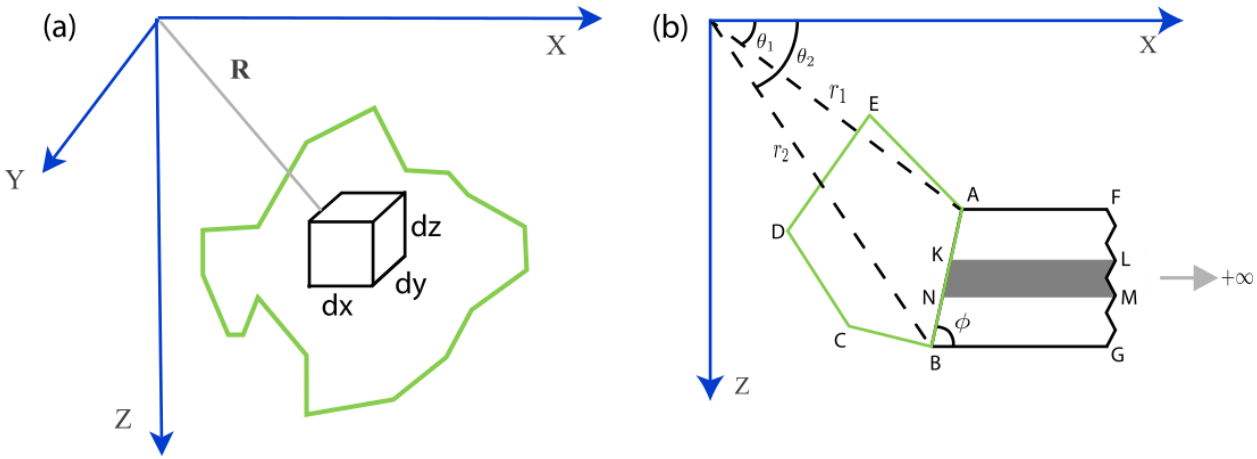

Figure 2.2. a) A volume element with dimension dx, dy, dz within an irregular shaped body. b) AFGBA is a semi-infinite prism containing a rod (KLMNK) that extends to positive infinity. ABCDEA is an arbitrary polygon defined along the edge of AB. Modified from Talwani (1965).

The magnetic potential, Ω, at the origin is given by:

$$\Omega = \frac{\vec{m} \cdot \vec{R}}{4\pi R^3} \tag{2.4}$$

where *m* is the magnetic moment of the volume element and R is the distance from the origin (Figure 2.2A).

Assuming that this volume element contains a uniform intensity of magnetization, J, the magnetic moment of a body can be represented as:

$$\vec{m} = \vec{J}dxdydz \tag{2.5}$$

The magnetic moment in terms of Cartesian coordinates x, y, z, can be written as:

$$\Omega = \frac{J_x x + J_y y + J_z z}{4\pi(x^2 + y^2 + z^2)^{3/2}} dxdydz \tag{2.6}$$

Using the assumption that the body extends from negative infinity to positive infinity in the y-direction and then integrating equation 2.6 with respect to y, the magnetic potential has the form:

$$\Omega = \int_{-\infty}^{\infty} \frac{J_x x + J_y y + J_z z}{4\pi(x^2 + y^2 + z^2)^{3/2}} dy = \frac{(J_x x + J_z z)}{2\pi(x^2 + z^2)} dxdz \tag{2.7}$$

The vertical (V) and horizontal (H) components of the magnetic strength can be derived by differentiating equation (2.7) with respect to z and x respectively and results in the following equations results in the following equations:

$$V = -\frac{\partial \Omega}{\partial z} = \frac{2J_x xz - J_z(x^2 - z^2)}{2\pi(x^2 + z^2)^2} dxdz \tag{2.8}$$

$$H = -\frac{\partial \Omega}{\partial x} = \frac{2J_z xz + J_x(x^2 - z^2)}{2\pi(x^2 + z^2)^2} dxdz \tag{2.9}$$

Assuming that the body extents to positive infinity in the x-direction we can simplify equations (2.8) and (2.9) by integrating from x to positive infinity, which results in:

$$V = \int_x^{\infty} \frac{2J_x xz - J_z(x^2 - z^2)}{2\pi(x^2 + z^2)^2} dxdz = \frac{J_x z - J_z x}{2\pi(x^2 + z^2)} dz \tag{2.10}$$

$$H = \int_x^{\infty} \frac{2J_z xz + J_x(x^2 - z^2)}{2\pi(x^2 + z^2)^2} dxdz = \frac{J_x x - J_z z}{2\pi(x^2 + z^2)} dz \tag{2.11}$$

Equations (2.10) and (2.11) are the components produced by the rod KLMNK in Figure 2.2b. The resulting integrating these equations from z_1 to z_2, the magnetic field strength for the prism AFGBA in Figure 2.2b produces equations that can be expressed in the simplified form as shown below (see detailed step by step derivation in the Supporting Information file):

$$V = \frac{1}{2\pi}(J_x Q - J_z P) \tag{2.12}$$

$$H = \frac{1}{2\pi}(J_z Q + J_x P) \tag{2.13}$$

where,

$$Q = \gamma_z^2 \, ln\left(\frac{r_2}{r_1}\right) - \delta\gamma_z\gamma_x(\alpha_2 - \alpha_1) \tag{2.14}$$

$$P = \gamma_z\gamma_x \, ln\left(\frac{r_2}{r_1}\right) + \delta\gamma_z^2(\alpha_2 - \alpha_1) \tag{2.15}$$

$$\gamma_z = \frac{z_{21}}{\sqrt{x_{21}^2 + z_{21}^2}} \tag{2.16}$$

$$\gamma_x = \frac{x_{21}}{\sqrt{x_{21}^2 + z_{21}^2}} \tag{2.17}$$

$$r_1 = \sqrt{x_1^2 + z_1^2} \tag{2.18}$$

$$r_2 = \sqrt{x_2^2 + z_2^2} \tag{2.19}$$

$$\alpha_1 = tan^{-1}\left(\frac{\delta(z_1 + gx_1)}{x_1 - gz_1}\right) \tag{2.20}$$

$$\alpha_2 = tan^{-1}\left(\frac{\delta(z_2 + gx_2)}{x_2 - gz_2}\right) \tag{2.21}$$

$$g = \frac{x_2 - x_1}{z_2 - z_1} = \frac{x_{21}}{z_{21}} \tag{2.22}$$

$\delta = 1$ if $x_1 > gz_1, \delta = -1$ if $x_1 < gz_1$

For an arbitrarily shaped polygon a point x_i, z_i represents a corner of the polygon and a point x_{i+1}, z_{i+1} to be the next corner of the polygon. Equations (2.12) and (2.13) represent the magnetic strength of the rectangular region AFGBA for only one side of the polygon. For a polygon with n-sides there is a n number of prisms of the same form as AFGBA. Calculation for a positive anomaly requires calculation of the polygon clockwise with reference to the origin as depicted in Figure 2.4 and summing the contribution of each side.

To evaluate the total intensity anomaly, T, we need to sum the projection of H and V along the direction of the total field. This can be done by manipulating the magnetization vectors associated with total magnetization (J) while using the convention shown in Figure 2.3. In general, total magnetization is a superposition of induced (J_i) and remnant magnetization (J_r) which are given by:

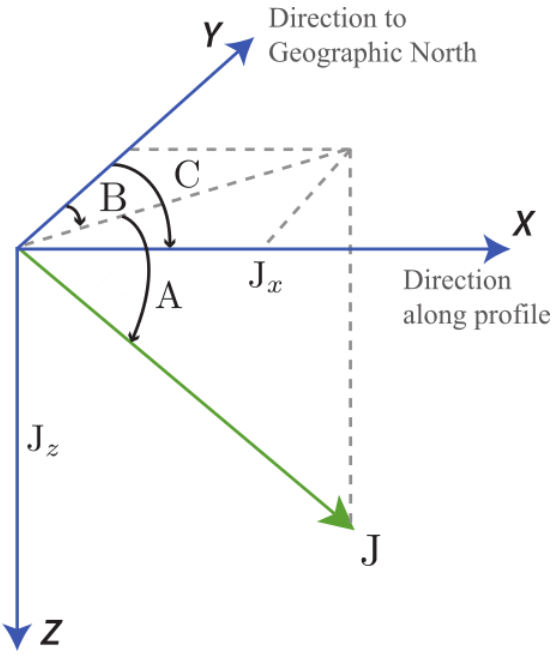

Figure 2.3. Modified from Talwani (1965). J is the total magnetization direction and J_x and J_z are the vector components with X,Y and Z being the cardinal directions with +Z being directed down. A is the angle that defines the horizontal projection of J. B is the angle measured from the geographic north clockwise towards the horizontal projection of J. C is the angle between geographic north and the positive x-axis.

$$\vec{J}_i = J_i(\cos I \cos D \ \hat{n} + \cos I \sin D \ \hat{e} + \sin I \ \hat{v}) \tag{2.23}$$

$$\vec{J}_r = J_r(\cos I_r \cos D_r \ \hat{n} + \cos I_r \sin D_r \ \hat{e} + \sin I_r \ \hat{v}) \tag{2.24}$$

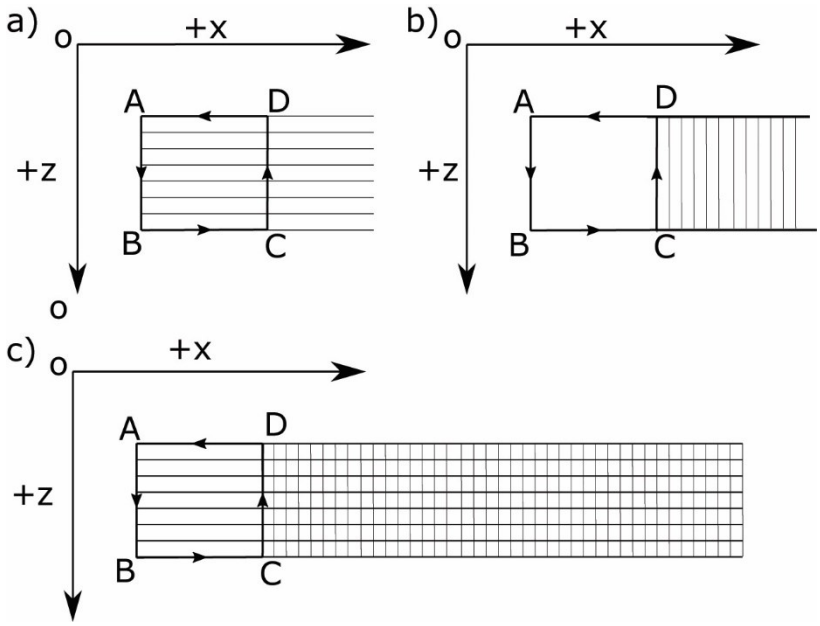

Figure 2.4. Visualization of the order of calculation of the magnetic field for a square ABCDA. Sides DA and CB provide no contribution as z2 – z1 = 0. (a) AB provides a positive contribution in the direction of the line integral with the horizontal lines shading the area of the semiinfinite prism. (b) CD provides a negative contribution in the direction of the line integral with the vertical lines shading the area of the semiinfinite prism. (c) Summation of the contributions from all sides results in only the magnetic field from the space enclosed in ABCDA, the area that has both horizontal and vertical lines cancel out.

where $\hat{n}$ = north, $\hat{e}$= east, $\hat{v}$= vertical, I = induced inclination, D = induced declination, I_r = remnant inclination, D_r = remnant declination. Using equations (2.23) and (2.24) the angle (Δ) between the two vectors can be determined as follows:

$$\Delta = cos^{-1}\left(\frac{\vec{J}_i \cdot \vec{J}_r}{J_i J_r}\right) \tag{2.25}$$

$$\Delta = cos^{-1}\left(\hat{J}_i \cdot \hat{J}_r\right) \tag{2.26}$$

$$\Delta = cos^{-1}(cos\, I\ cos\, D\ cos\, I_r\ cos\, D_r + cos\, I\ sin\, D\ cos\, I_r\ sin\, D_r + sin\, I\ sin\, I_r) \tag{2.27}$$

This angle Δ can be used to calculate the magnitude of the total magnetization (J) as well as its inclination (A) and declination (B). Using the cosine law the total magnetization J is defined as:

$$J^2 = J_i^2 + J_r^2 - 2J_i\, J_r\, cos\, \Delta \tag{2.28}$$

To determine the inclination (A) and declination (B) of J we split J_i and J_r into their horizontal (J_{iH} and J_{rH}, respectively) and vertical components (J_{iV} and J_{rV}, respectively). Inclination is then derived as follows:

$$J_V = J_{iV} + J_{rV} \tag{2.29}$$

$$J_V = J_i\, sin\, I + J_r\, sin\, I_r \tag{2.30}$$

$$J\, sin\, A = J_i\, sin\, I + J_r\, sin\, I_r \tag{2.31}$$

$$sin\, A = \frac{J_i\, sin\, I + J_r\, sin\, I_r}{J} \tag{2.32}$$

$$A = sin^{-1}\left(\frac{J_i\, sin\, I + J_r\, sin\, I_r}{J}\right) \tag{2.33}$$

Similarly, declination it derived as follows:

$$J_H = J\, cos\, A \tag{2.34}$$

$$J_H = J_{iH} + J_{rH} \tag{2.35}$$

$$J_H = J_i \cos I + J_r \cos I_r \tag{2.36}$$

$$J_H \hat{n} = J_H \cos B \tag{2.37}$$

$$J_H \cos B = J_{iH} \hat{n} + J_{rH} \hat{n} \tag{2.38}$$

$$J_H \cos B = J_{iH} \cos D + J_{rH} \cos D_r \tag{2.39}$$

$$J_H \cos B = J_i \cos I \cos D + J_r \cos I_r \cos D_r \tag{2.40}$$

$$\cos B = \frac{J_i \cos I \cos D + J_r \cos I_r \cos D_r}{J_H} \tag{2.41}$$

$$B = \cos^{-1}\left(\frac{J_i \cos I \cos D + J_r \cos I_r \cos D_r}{J \cos A}\right) \tag{2.42}$$

The intensity of magnetization of magnetization in the x and z directions in the terms of total magnetization, J, in terms of A, B, C can be defined as:

$$J_x = J \cos(A) \cos(C - B) \tag{2.43}$$

$$J_z = J \sin(A) \tag{2.44}$$

The total intensity anomaly (T) can then be defined as:

$$T = V \sin(A) + H \cos(A) \cos(C - B) \tag{2.45}$$

2.4. Discussion

Upon a rederivation of the original Talwani and Heirtzler (1964) algorithm we found three explicit differences and errors in Talwani and Heirtzler's (1964) derivation. The first error began in the definition of x. Figure 2.5 demonstrates the resultant difference between the two expressions for a polygon. Continuing derivation of the magnetic fields using Talwani and Heirtzler (1964) definition for x, it was evident that the definition for θ_1 and θ_2 are not equivalent to the angle the corners of the side make with the origin as depicted in Figure 2.2a. The final issue found in derivation was the definition of a δ term. In Talwani and Heirtzlers (1964) this term was assumed to value 1, indicating that they did not account for the impact of the absolute value in the derivation.

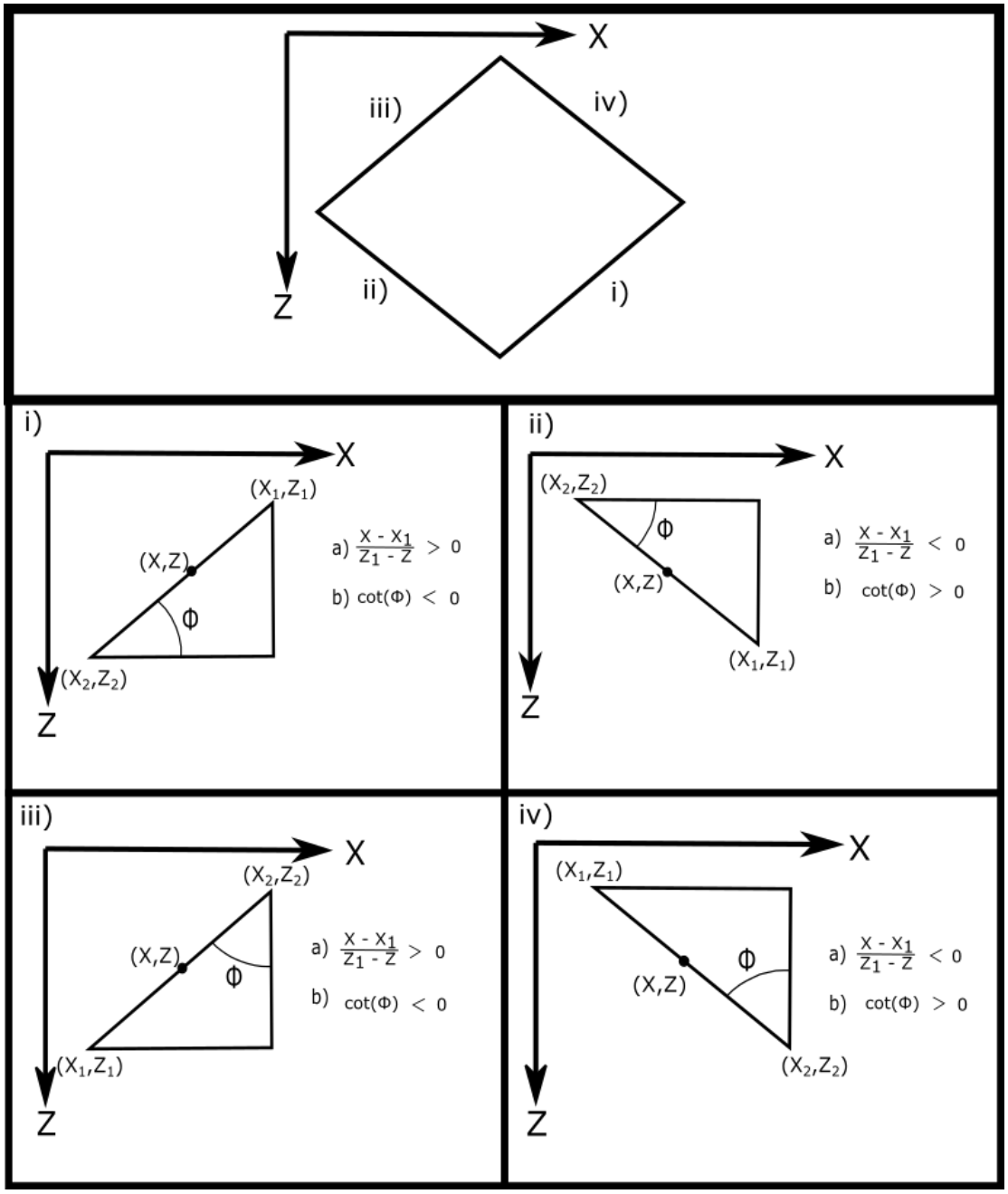

Figure 2.5. Depiction of a simple polygon shape (top) and the resulting values of $\cot(\phi)$ in our derivation (a) and in Talwani and Heirtzler (1964) definition of $\cot(\phi)$ (b) for each side respectively. The figure demonstrates that the correct calculation for $\cot(\phi)$ has an opposite sign of Talwani and Heirtzler's (1964) definition for this object.

Due to the many different shapes and sizes of polygons the resultant error is not broadly quantifiable but dependent on shape of the polygon, and inclination/declination of the induced

magnetic field. To demonstrate the potential differences produced by different derivations, we have calculated the induced magnetic field produced from a diamond with three different inclinations and compare also with the method of Won and Bevis (1987). The method of Won and Bevis (1987) who derived the magnetic anomaly due to a polygonal cylinder in a similar matter to ours but using references to vertex coordinates to reduce references to angular quantities and trigonometric identities. Figure 2.6 illustrates the comparison of the magnetic anomalies computed using the six different algorithms: (i) Talwani and Heirtzler (1964), (ii) our rederivation using Talwani and Heirtzlers (1964) definition of x and accounting for corrected δ, (iii) definition of x and corrected θ, (iv) definition of x and accounting for the corrected δ and θ term, (v) robust derivation from first principles, and (vi) Won and Bevis (1987). We find that the results for (i), (v) and (iv) are very similar. The errors inherent in the original derivation of Talwani and Heirtzler (1964), particularly the definitions of θ_1, θ_2 and δ, by removal compensate for each other to produce results that approximately agree with the properly derived solution provided by our derivation. However, when the corrections for θ_1, θ_2 and δ are applied independently they produce the same incorrect anomaly, which indicates that these errors had to be made dependently otherwise it would produce incorrect anomalies. We recommend the solution produced by Talwani and Heirtzler (1964) be avoided, as it cannot be guaranteed to work for all possible shapes and cases. It is, however, clear that the errors were fundamental and that when corrected the original algorithm of Talwani and Heirtzler (1964) produced significant differences in the modeled magnetic field (see Supporting Information file).

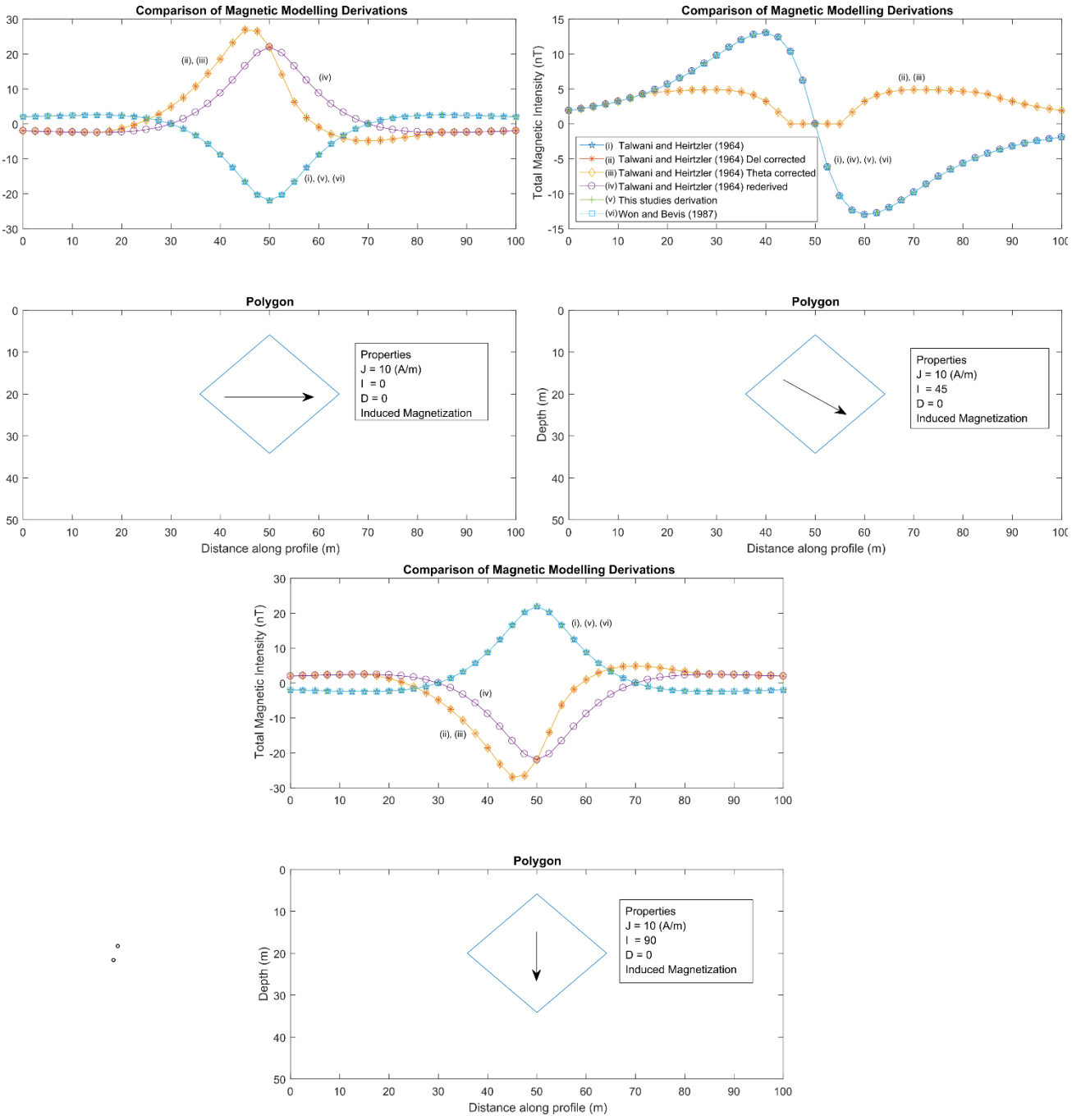

Figure 2.6. Comparison of the total magnetic intensity of a diamond at a magnetic inclination of 0°, 45°, and 90° of (i) Talwani and Heirtzler (1964), (ii) our rederivation using Talwani and Heirtzler's (1964) definition of x and accounting for corrected δ, (iii) definition of x and corrected θ, (iv) definition of x and accounting for the corrected δ and θ term, (v) our robust derivation in this study from first principles, and (vi) Won and Bevis (1987). The magnetization of the objects is 10 A/m. The original Talwani and Heirtzler (1964) algorithm produces results similar to this study algorithm and Won and Bevis (1987) algorithm in this example and a few other cases we have tried, although it cannot be guaranteed to work for all possible shapes and cases. The Talwani and Heirtzler (1964) rederived algorithm with the different corrections

applied together and independently produces offset results when calculated to a diamond for different inclinations.

2.5. Conclusions

The resulting expressions for the components of the magnetic field (2.12, 2.13) are not equal to the expressions derived by Talwani and Heirtzler (1964). The discrepancy between our derivation and Talwani and Heirtzler (1964) lies in the definition of the variable x, definition of the angles θ_1 and θ_2, and the dismissal of an absolute value. Talwani and Heirtzler (1964) have erroneous definitions. Detailed rederivation of Talwani and Heirtzler formulas to calculate magnetic anomalies caused by two dimensional structures of arbitrary shape is given in the appendix. The rederived final solution is different from the original published formulas of Talwani and Heirtzler (1964) and produces incorrect anomalies (Figure 2.5), therefore we strongly recommend to use our algorithm derived in this study to avoid any fundamental errors in calculating the anomalies.

Software and data availability

The free software and example data are available for download from www.ualberta.ca/~vadim/software.htm. This publication has to be referred with any use of the software.

Acknowledgment

We are thankful K. Bianchi for his help with derivation confirmation, S. Alhashwa for his help at the initial stage of the project and F. Caratori Tontini for his in-depth verification of our derivations and discussion that led to essential improvement of this manuscript. The project was funded by the Natural Sciences and Engineering Research Council of Canada of V.A.K. (NSERC grant RGPIN-2019-04780). This study forms part of B.L. M.Sc. thesis at the University of Alberta.

References

Jeshvaghani, M. S., & Darijani, M. (2014). Two-dimensional geomagnetic forward modeling using adaptive finite element method and investigation of the topographic effect. Journal of Applied Geophysics, 105, 169-179.

Kostrov, N. P. (2007). Calculation of magnetic anomalies caused by 2D bodies of arbitrary shape with consideration of demagnetization. Geophysical prospecting, 55(1), 91-115.

Lelievre, P.G., & Oldenburg, D.W. (2006). Magnetic forward modelling and inversion for high susceptibility. Geophysical Journal International, 166 (1), 76-90.

Talwani, M., & Heirtzler, J. R., 1962. The Mathematical Expression for the Magnetic Anomaly over a Two-Dimensional Body of Polygonal Cross Section. Lamont Doherty Geol. Obs. Columbia Univ., Tech. Rep. 6.

Talwani, M., & Heirtzler, J. R., 1964. Computation of magnetic anomalies caused by two dimensional structures of arbitrary shape. *Computers in the mineral industries*, part 1: Stanford University publications, Geol. Sciences, 9, 464-480.

Talwani, M. (1965). Computation with the help of a digital computer of magnetic anomalies caused by bodies of arbitrary shape. Geophysics, 30(5), 797-817.

Won, I. J., & Bevis, M. (1987). Computing the gravitational and magnetic anomalies due to a polygon: Algorithms and Fortran subroutines. Geophysics, 52(2), 232-238.

2.6 Appendix

2.6.1 Detailed derivation of the formulas to calculate magnetic anomalies caused by two dimensional structures of arbitrary shape

Consider that there exists an elemental volume contained within an irregularly shaped body. This elemental volume extends from negative to positive infinity in the y-direction. Bodies of irregular shapes can be approximated by a polygon, which can be and reduced to solving semi-infinite two-dimensional polygons (Talwani and Heirtzler, 1964). Now consider a small volume element with dimensions dx, dy, dz (Figure 2.1A) and its properties.

The magnetic potential, Ω, at the origin is given by:

$$\Omega = \frac{\vec{m} \cdot \vec{R}}{4\pi R^3} \tag{2.46}$$

where m is the magnetic moment of the volume element and R is the distance from the origin (Figure 2.2A).

Assuming that this volume element contains a uniform intensity of magnetization, J, the magnetic moment of a body can be represented as:

$$\vec{m} = \vec{J} dx dy dz \tag{2.47}$$

The magnetic moment in terms of Cartesian coordinates x, y, z, can then be written as:

$$\Omega = \frac{J_x x + J_y y + J_z z}{4\pi(x^2 + y^2 + z^2)^{3/2}} dxdydz \tag{2.48}$$

Using the assumption that the body extends from negative infinity to positive infinity in the y-direction and then integrating equation 3 with respect to y, the magnetic potential has the form

$$\Omega = \int_{-\infty}^{\infty} \frac{J_x x + J_y y + J_z z}{4\pi(x^2 + y^2 + z^2)^{3/2}} dy = \frac{(J_x x + J_z z)}{2\pi(x^2 + z^2)} dxdz \tag{2.49}$$

The vertical (V) and horizontal (H) components of the magnetic strength can be derived by differentiating equation (2.49) with respect to z and x respectively, and results in the following equations:

$$V = -\frac{\partial \Omega}{\partial z} = \frac{2J_x xz - J_z(x^2 - z^2)}{2\pi(x^2 + z^2)^2} dxdz \tag{2.50}$$

$$H = -\frac{\partial \Omega}{\partial x} = \frac{2J_z xz + J_x(x^2 - z^2)}{2\pi(x^2 + z^2)^2} dxdz \tag{2.51}$$

Assuming that the body extents to positive infinity in the x-direction we can simplify equations (5) and (6) by integrating from x to positive infinity, which results in:

$$V = \int_{x}^{\infty} \frac{2J_x xz - J_z(x^2 - z^2)}{2\pi(x^2 + z^2)^2} dxdz = \frac{J_x z - J_z x}{2\pi(x^2 + z^2)} dz \tag{2.52}$$

$$H = \int_{x}^{\infty} \frac{2J_z xz + J_x(x^2 - z^2)}{2\pi(x^2 + z^2)^2} dxdz = \frac{J_x x - J_z z}{2\pi(x^2 + z^2)} dz \tag{2.53}$$

Equations (2.52) and (2.53) are the components produced by the rod KLMNK in Figure 2.1B. Integrating these equations from z_1 to z_2, the magnetic field strength for the prism AFGBA in Fig. 1B can be calculated.

$$V = \int_{z1}^{z2} \frac{J_x z - J_z x}{2\pi(x^2 + z^2)} dz \tag{2.54}$$

In order to compute this integral, consider taking a point on the side of a polygon (ABCDEA) that makes up the region of interest (AFGBA). This enables us to find x as a function of the coordinates of the corners and z.

Let

$$g = \frac{z_2 - z_1}{x_2 - x_1} = \frac{x - x_1}{z - z_1} \tag{2.55}$$

Equation (2.55) can then be rearranged into,

$$x = g(z - z_1) + x_1 \tag{2.56}$$

and then inserted into equation (2.54), which results in the following sets of equations,

$$V = \frac{1}{2\pi}\int_{z1}^{z2} \frac{J_x z - J_z(g(z - z_1) + x_1)}{[g(z - z_1) + x_1]^2 + z^2}\,dz \tag{2.57}$$

$$V = \frac{1}{2\pi}\int_{z1}^{z2} \frac{(J_x z - gJ_z)z - J_z(x_1 - gz_1)}{(1 + g^2)z^2 + 2g(x_1 - gz_1)z + (x_1 - gz_1)^2}\,dz \tag{2.58}$$

We can rewrite this in simpler terms by letting

$$a = 1 + g^2 \tag{2.59}$$

$$b = 2g(x_1 - gz_1)z \tag{2.60}$$

$$c = (x_1 - gz_1)^2 \tag{2.61}$$

which results in,

$$V = \frac{1}{2\pi}\int_{z1}^{z2} \frac{(J_x - gJ_z)z - J_z(x_1 - gz_1)}{az^2 + bz + c}\,dz \tag{2.62}$$

These equations can be rewritten in terms of to 2 components,

$$V = \frac{1}{2\pi}\int_{z1}^{z2} \frac{(J_x - gJ_z)z}{az^2 + bz + c}\,dz - \frac{1}{2\pi}\int_{z1}^{z2} \frac{J_z(x_1 - gz_1)}{az^2 + bz + c}\,dz \tag{2.63}$$

$$V = \frac{(J_x - gJ_z)}{2\pi}\int_{z1}^{z2}\frac{z}{az^2+bz+c}dz - \frac{J_z(x_1 - gz_1)}{2\pi}\int_{z1}^{z2}\frac{dz}{az^2+bz+c} \tag{2.64}$$

$$V = I_1 + I_2 \tag{2.65}$$

where,

$$I_1 = \frac{(J_x - gJ_z)}{2\pi}\int_{z1}^{z2}\frac{z}{az^2+bz+c}dz \tag{2.66}$$

$$I_2 = -\frac{J_z(x_1 - gz_1)}{2\pi}\int_{z1}^{z2}\frac{dz}{az^2+bz+c} \tag{2.67}$$

Equation (2.65) can be integrated using the following integral identities:

For:

$$A \neq 0 \tag{2.68}$$

$$4AC - B^2 > 0 \tag{2.69}$$

$$\int \frac{xdx}{Ax^2+Bx+C} = \frac{1}{2A}ln|Ax^2+Bx+C| - \frac{B}{A\sqrt{4AC-B^2}}tan^{-1}\left(\frac{2Ax+B}{\sqrt{4AC-B^2}}\right)$$

$$\int \frac{dx}{Ax^2+Bx+C} = \frac{2}{\sqrt{4AC-B^2}}tan^{-1}\left(\frac{2Ax+B}{\sqrt{4AC-B^2}}\right) \tag{2.70}$$

To use these identities, we first check that the criteria are met for equation (2.68). First by checking that $A \neq 0$. For the first criteria, equation (12) defines $= 1 + g^2$, which requires that $A > 0$, which implies $A \neq 0$.

Checking $4AC - B^2 > 0$ is done as follows:

$$B = 2g(x_1 - gz_1) \tag{2.71}$$

$$C = x_1 - gz_1 \tag{2.72}$$

$$4AC - B^2 = 4(1 + g^2)(x_1 - gz_1)^2 - \big(2g(x_1 - gz_1)\big)^2 \tag{2.73}$$

$$4AC - B^2 = 4(1 + g^2)(x_1 - gz_1)^2 - 4g^2(x_1 - gz_1))^2$$
$$4AC - B^2 = (x_1 - gz_1)^2(4(1 + g^2) - 4g^2)$$
$$4AC - B^2 = (x_1 - gz_1)^2(4(1 + g^2) - 4g^2)$$
$$4AC - B^2 = (x_1 - gz_1)^2(4(1 + g^2 - g^2)$$
$$4AC - B^2 = 4(x_1 - gz_1)^2 \tag{2.74}$$

Since both criteria are met, we use the above identities to solve for I_1 and I_2.

$$I_1 = \frac{J_x - gJ_z}{2\pi}\left[\begin{matrix}\frac{1}{2a}(ln|az_2^2 + bz_2 + c| - ln|az_1^2 + bz_1 + c|) \\ -\frac{b}{a\sqrt{4ac - b^2}}\left(tan^{-1}\left(\frac{2az_2 + b}{\sqrt{4ac - b^2}}\right) - tan^{-1}\left(\frac{2az_1 + b}{\sqrt{4ac - b^2}}\right)\right)\end{matrix}\right] \tag{2.75}$$

where,

$$az_2^2 + bz_2 + c = (1 + g^2)z_2^2 + 2g(x_1 - gz_1)z_2 + (x_1 - gz_1)^2$$

$$az_2^2 + bz_2 + c = z_2^2 + g^2z_2^2 + 2gx_1z_2 - 2g^2z_1z_2 + x_1^2 + g^2z_1^2 - 2gx_1z_1$$

$$az_2^2 + bz_2 + c = z_2^2 + g^2(z_2^2 - 2z_1z_2 + z_1^2) + 2gx_1z_2 - 2gx_1z_1 + x_1^2$$

$$az_2^2 + bz_2 + c = z_2^2 + g^2(z_2 - z_1)^2 + 2gx_1z_2 - 2gx_1z_1 + x_1^2$$

$$az_2^2 + bz_2 + c = z_2^2 + g^2(z_2 - z_1)^2 + 2gx_1(z_2 - z_{1)} + x_1^2$$

but, $g(z_2 - z_1) = x_2 - x_1$, which then gives,

$$az_2^2 + bz_2 + c = z_2^2 + (x_2 - x_1)^2 + 2x_1(x_2 - x_1) + x_1^2 = z_2^2 + x_2^2 \quad (2.76)$$

Similarly,

$$az_1^2 + bz_1 + c = z_1^2 + x_1^2 \quad (2.77)$$

By inspection of Figure 2.1B, the following relationship exists:

$$r_1^2 = z_1^2 + x_1^2 = az_1^2 + bz_1 + c \quad (2.78)$$

$$r_2^2 = z_2^2 + x_2^2 = az_2^2 + bz_2 + c \quad (2.79)$$

By inspection equation 2.79 is equivalent to its absolute value:

$$r_1^2 = |az_1^2 + bz_1 + c| = |r_1^2| \quad (2.80)$$

$$r_2^2 = |az_2^2 + bz_2 + c| = |r_2^2| \quad (2.81)$$

therefore,

$$ln|az_1^2 + bz_1 + c| = ln|r_1^2| = ln\, r_1^2 \tag{2.82}$$

$$ln|az_2^2 + bz_2 + c| = ln|r_2^2| = ln\, r_2^2 \tag{2.83}$$

The terms $2az_{1,2} + b$ in equation (2.75) can be rewritten as follows:

$$2az_2 + b = 2(g^2 + 1)z_2 + 2g(x_1 - gz_1)$$
$$2az_2 + b = 2g^2 z_2 + 2z_2 + 2gx_1 - 2g^2 z_1$$
$$2az_2 + b = 2g^2(z_2 - z_1) + 2z_2 + 2gx_1$$

recall $g(z_2 - z_1) = x_2 - x_1$, so that,

$$2az_2 + b = 2g(x_2 - x_1) + 2z_2 + 2gx_1 = 2(z_2 + gx_2) \tag{2.84}$$

similarly,

$$2az_1 + b = 2(z_1 + gx_1) \tag{2.85}$$

(17)

The term $\sqrt{4ac - b^2}$is rewritten as follows:

$$\sqrt{4ac - b^2} = \sqrt{4(1 + g^2)(x_1 - gz_1)^2 - (2g(x_1 - gz_1))^2}$$
$$\sqrt{4ac - b^2} = \sqrt{4(x_1 - gz_1)^2(1 + g^2 - g^2)}$$
$$\sqrt{4ac - b^2} = 2\sqrt{(x_1 - gz_1)^2}$$

$$\sqrt{4ac - b^2} = 2|x_1 - gz_1| \tag{2.86}$$

$$\sqrt{4ac - b^2} = 2\delta(x_1 - gz_1) \tag{2.87}$$

where, $\delta = 1$ if $x_1 > gz_1, \delta = -1$ if $x_1 < gz_1$

Substituting equations (2.84), (2.85), (2.87), into equation (2.75), produces:

$$I_1 = \frac{J_x - gJ_z}{2\pi}\left[\frac{1}{2(1+g^2)}(ln\, r_2^2 - ln\, r_1^2) - \frac{2g(x_1 - gz_1)}{2(1+g^2)\delta(x_1 - gz_1)}\begin{pmatrix} tan^{-1}\left(\frac{2(z_2 + gx_2)}{2\delta(x_1 - gz_1)}\right) \\ - tan^{-1}\left(\frac{2(z_1 + gx_1)}{2\delta(x_1 - gz_1)}\right)\end{pmatrix}\right] \tag{2.88}$$

recall that, $g = \frac{x_2 - x_1}{z_2 - z_1} \Rightarrow g(z_2 - z_1) = x_2 - x_1 \Rightarrow x_1 - gz_1 = x_2 - gz_2$, which can be substituted into the above equation to produce:

$$I_1 = \frac{J_x - gJ_z}{2\pi}\left[\frac{1}{2(1+g^2)} ln\left(\frac{r_2}{r_1}\right)^2 - \frac{\delta g}{(1+g^2)}\left(tan^{-1}\left(\frac{\delta(z_2 + gx_2)}{(x_2 - gz_2)}\right) - tan^{-1}\left(\frac{\delta(z_1 + gx_1)}{(x_1 - gz_1)}\right)\right)\right] \tag{2.89}$$

$$I_1 = \frac{J_x - gJ_z}{2\pi}\left[\frac{1}{2(1+g^2)} ln\left(\frac{r_2}{r_1}\right)^2 - \frac{\delta g}{(1+g^2)}(tan^{-1}(A_2) - tan^{-1}(A_1))\right] \tag{2.90}$$

where, $A_1 = \frac{\delta(z_1 + gx_1)}{(x_1 - gz_1)}$ and $A_2 = \frac{\delta(z_2 + gx_2)}{(x_2 - gz_2)}$

$$I_1 = \frac{J_x - gJ_z}{2\pi}\left[\frac{1}{2(1+g^2)} ln\left(\frac{r_2}{r_1}\right)^2 - \frac{\delta g}{(1+g^2)}(\alpha_2 - \alpha_1)\right] \tag{2.91}$$

where, $\alpha_1 = tan^{-1}(A_1)$ and $\alpha_2 = tan^{-1}(A_2)$

Now solving for I_2,

$$I_2 = \frac{-(J_z(x_1 - gz_1))}{2\pi}\int_{z_1}^{z_2} \frac{dz}{az^2 + bz + c} = \frac{2}{\sqrt{4AC - B^2}} tan^{-1}\left(\frac{2Ax + B}{\sqrt{4AC - B^2}}\right) \tag{2.92}$$

Using equations (2.84), (2.85), (2.87) as well as the appropriate integral identity we define:

$$I_2 = \frac{-(J_z(x_1 - gz_1))}{2\pi}\left[\frac{2}{\sqrt{4ac - b^2}} tan^{-1}\left(\frac{2az + b}{\sqrt{4ac - b^2}}\right)\right]_{z_1}^{z_2}$$

$$I_2 = \frac{-(J_z(x_1 - gz_1))}{2\pi}\left[\frac{2}{\sqrt{4ac - b^2}}\left(tan^{-1}\left(\frac{2az_2 + b}{\sqrt{4ac - b^2}}\right) - tan^{-1}\left(\frac{2az_1 + b}{\sqrt{4ac - b^2}}\right)\right)\right]$$

$$I_2 = \frac{-(J_z(x_1 - gz_1))}{2\pi}\left[\frac{2}{2\delta(x_1 - gz_1)}(tan^{-1}(A_2) - tan^{-1}(A_1))\right]$$

$$I_2 = \frac{-(J_z(x_1 - gz_1))}{2\pi}\left[\frac{1}{\delta(x_1 - gz_1)}(\alpha_2 - \alpha_1)\right]$$

$$I_2 = \frac{-J_z\delta}{2\pi}(\alpha_2 - \alpha_1) \tag{2.93}$$

From equation (2.91) and (2.93), we can define V as:

$V = I_1 + I_2$

$$V = \frac{J_x - gJ_z}{2\pi}\left[\frac{1}{1+g^2} ln\left(\frac{r_2}{r_1}\right) - \frac{\delta g}{(1+g^2)}(\alpha_2 - \alpha_1)\right] - \frac{J_z \delta}{2\pi}(\alpha_2 - \alpha_1) \tag{2.94}$$

Recall that $g = \frac{x_2 - x_1}{z_2 - z_1}$, then by letting $x_{21} = x_2 - x_1$and $z_{21} = z_2 - z_1$allows g to be defined as $g = \frac{x_{21}}{z_{21}}$ which produces:

$$V = \frac{z_{21}}{2\pi\sqrt{x_{21}^2 + z_{21}^2}}\left[\begin{matrix} J_x\left(\frac{z_{21}}{\sqrt{x_{21}^2 + z_{21}^2}} ln\left(\frac{r_2}{r_1}\right) - \frac{\delta x_{21}}{\sqrt{x_{21}^2 + z_{21}^2}}(\alpha_2 - \alpha_1)\right) \\ -J_z\left(\frac{x_{21}}{\sqrt{x_{21}^2 + z_{21}^2}} ln\left(\frac{r_2}{r_1}\right) - \frac{\delta z_{21}}{\sqrt{x_{21}^2 + z_{21}^2}}(\alpha_2 - \alpha_1)\right)\end{matrix}\right] \tag{2.95}$$

Solving for the horizontal component (H) can be done in a similar manner. Starting with equation (2.53) we integrate with respect to z to obtain:

$$H = \frac{1}{2\pi}\int_{z_1}^{z_2} \frac{J_x x + J_z z}{x^2 + z^2}\, dz \tag{2.96}$$

Recall that we defined$x = (z - z_1)g + x_1$, so subbing in this definition yields:

$$H = \frac{1}{2\pi}\int_{z_1}^{z_2} \frac{J_x\big((z-z_1)g + x_1\big) + J_z z}{\big((z-z_1)g + x_1\big)^2 + z^2}\,dz \tag{2.97}$$

which can then be split into two terms:

$$H = \frac{1}{2\pi}\int_{z_1}^{z_2} \frac{(J_z + gJ_x)z}{az^2 + bz + c}\,dz + \frac{1}{2\pi}\int_{z_1}^{z_2} \frac{J_x(x_1 - gz_1)}{az^2 + bz + c}\,dz \tag{2.98}$$

This can be written in short form using the following terms:

$$I_{1H} = \frac{J_z + gJ_x}{2\pi}\int_{z_1}^{z_2} \frac{z}{az^2 + bz + c}\,dz \tag{2.99}$$

$$I_{2H} = \frac{J_z + gJ_x}{2\pi}\int_{z_1}^{z_2} \frac{z}{az^2 + bz + c}\,dz \tag{2.100}$$

$$H = I_{1H} + I_{2H} \tag{2.101}$$

Using the appropriate identities we can integrate equation (2.98). For the first term integration yields:

$$I_{1H} = \frac{J_z + gJ_x}{2\pi}\left[\begin{matrix}\frac{1}{2a}\left(ln|az_2^2 + bz_2 + c| - ln|az_1^2 + bz_1 + c|\right) \\ -\frac{b}{a\sqrt{4ac - b^2}}\left(tan^{-1}\left(\frac{2az_2 + b}{\sqrt{4ac - b^2}}\right) - tan^{-1}\left(\frac{2az_1 + b}{\sqrt{4ac - b^2}}\right)\right)\end{matrix}\right] \tag{2.102}$$

By applying the same transformations used in earlier we can transform equation (2.102) into the following expression:

$$I_{1H} = \frac{J_z + gJ_x}{2\pi}\left[\frac{1}{1+g^2} ln\left(\frac{r_2}{r_1}\right) - \frac{\delta g}{1+g^2}(\alpha_2 - \alpha_1)\right] \tag{2.103}$$

The 2nd term $I_{2H} = \frac{J_x(x_1+gz_1)}{2\pi}\int_{z_1}^{z_2}\frac{dz}{az^2+bz+c}$ is a similar to equation (2.99) except the term that lies outside the integral, thus:

$$I_{2H} = \frac{J_x}{2\pi}\delta(\alpha_2 - \alpha_1) \tag{2.104}$$

Combining I_{1H} and I_{2H} yields:

$$H = \frac{J_z + gJ_x}{2\pi}\left[\frac{1}{1+g^2} ln\left(\frac{r_2}{r_1}\right) - \frac{\delta g}{1+g^2}(\alpha_2 - \alpha_1)\right] + \frac{J_x}{2\pi}\delta(\alpha_2 - \alpha_1) \tag{2.105}$$

Recalling that $x_{21} = x_2 - x_1$ and $z_{21} = z_2 - z_1$ allows g to be defined as in the following ways:

$$g = \frac{x_2 - x_1}{z_2 - z_1}$$

$$g = \frac{x_{21}}{z_{21}}$$

$$1 + g^2 = 1 + \left(\frac{x_{21}}{z_{21}}\right)^2 \tag{2.106}$$

Using these definitions produces:

$$H = \frac{z_{21}}{2\pi\sqrt{x_{21}^2 + z_{21}^2}}\left[\begin{array}{l} J_z\left(\frac{z_{21}}{\sqrt{x_{21}^2 + z_{21}^2}} ln\left(\frac{r_2}{r_1}\right) - \frac{\delta x_{21}}{\sqrt{x_{21}^2 + z_{21}^2}}(\alpha_2 - \alpha_1)\right) \\ +J_x\left(\frac{x_{21}}{\sqrt{x_{21}^2 + z_{21}^2}} ln\left(\frac{r_2}{r_1}\right) + \frac{\delta z_{21}}{\sqrt{x_{21}^2 + z_{21}^2}}(\alpha_2 - \alpha_1)\right) \end{array}\right] \tag{2.107}$$

A simplified form of Vertical and Horizontal expressions are as follows:

$$V = \frac{\gamma_z}{2\pi}\left[J_x\left(\gamma_z\, ln\left(\frac{r_2}{r_1}\right) - \delta\gamma_x(\alpha_2 - \alpha_1)\right) - J_z\left(\gamma_x\, ln\left(\frac{r_2}{r_1}\right) + \delta\gamma_z(\alpha_2 - \alpha_1)\right)\right] \tag{2.108}$$

$$H = \frac{\gamma_z}{2\pi}\left[J_z\left(\gamma_z\, ln\left(\frac{r_2}{r_1}\right) - \delta\gamma_x(\alpha_2 - \alpha_1)\right) + J_x\left(\gamma_x\, ln\left(\frac{r_2}{r_1}\right) + \delta\gamma_z(\alpha_2 - \alpha_1)\right)\right] \tag{2.109}$$

where,

$$\gamma_z = \frac{z_{21}}{\sqrt{x_{21}^2 + z_{21}^2}}$$

$$\gamma_x = \frac{x_{21}}{\sqrt{x_{21}^2 + z_{21}^2}}$$

$$r_1 = \sqrt{x_1^2 + z_1^2}$$

$$r_2 = \sqrt{x_2^2 + z_2^2}$$

$$\alpha_1 = tan^{-1}\left(\frac{\delta(z_1 + gx_1)}{x_1 - gz_1}\right)$$

$$\alpha_2 = tan^{-1}(\frac{\delta(z_2 + gx_2)}{x_2 - gz_2})$$

$$\delta = 1 \text{ if } x_1 > gz_1$$

$$\delta = -1 \text{ if } x_1 < gz_1$$

$$g = \frac{x_2 - x_1}{z_2 - z_1} = \frac{x_{21}}{z_{21}}$$

In a more simplified form our equations can be reduced to the following:

$$V = \frac{1}{2\pi}(J_x Q - J_z P) \tag{2.111}$$

$$H = \frac{1}{2\pi}(J_z Q + J_x P) \tag{2.112}$$

where,

$$Q = \gamma_z^2 \, ln\left(\frac{r_2}{r_1}\right) - \delta\gamma_z\gamma_x(\alpha_2 - \alpha_1) \tag{2.113}$$

$$P = \gamma_z\gamma_x \, ln\left(\frac{r_2}{r_1}\right) + \delta\gamma_z^2(\alpha_2 - \alpha_1) \tag{2.114}$$

For an arbitrarily shaped polygon a point x_i, z_i represents a corner of the polygon and a point x_{i+1}, z_{i+1} to be the next nearest corner of the polygon. Equations (2.113) and (2.114) represent the

magnetic strength of the rectangular region AFGBA for only one side of the polygon. For a polygon with n-sides there are a n number of prisms of the same form as AFGBA. By choosing the proper sign for each prism that comprise the polygon and summing their contribution of the magnetic field strength at the origin we can produce the magnetic anomaly for the entire polygon (AFGBA), at that point. Calculation for a positive anomaly requires calculation of the polygon clockwise with reference to the origin as depicted in Supporting Information Figure 2.1 and summing the contribution of each side.

To evaluate the total intensity anomaly, T, we need to sum the projection of H and V along the direction of the total field. This can be done by manipulating the magnetization vectors associated with total magnetization (J) while using the convention shown in Figure 2.2. In general, total magnetization is a superposition of induced (J_i) or remnant magnetization (J_r) which are given by:

$$\vec{J}_i = J_i(cos\, I\, cos\, D\, \hat{n} + cos\, I\, sin\, D\, \hat{e} + sin\, I\, \hat{v}) \tag{2.115}$$

$$\vec{J}_r = J_r(cos\, I_r\, cos\, D_r\, \hat{n} + cos\, I_r\, sin\, D_r\, \hat{e} + sin\, I_r\, \hat{v}) \tag{2.116}$$

where $\hat{n}$ = north, $\hat{e}$= east, $\hat{v}$= vertical, I = induced inclination, D = induced declination, I_r = remnant inclination, D_r = remnant declination. Using equations (2.115) and (2.116) the angle (Δ) between the two vectors can be determined as follows:

$$\Delta = cos^{-1}\left(\frac{\vec{J}_i \cdot \vec{J}_r}{J_i J_r}\right)$$

$$\Delta = cos^{-1}(\hat{J}_i \cdot \hat{J}_r)$$

$$\Delta = cos^{-1}(cos\, I\, cos\, D\, Cos I_r\, cos\, D_r + cos\, I\, sin\, D\, cos\, I_r\, sin\, D_r + sin\, I\, sin\, I_r) \tag{2.117}$$

This angle Δ can be used to calculate the magnitude of the total magnetization (J) as well as its inclination (A) and declination (B). Using the cosine law the total magnetization J is defined as:

$$J^2 = J_i^2 + J_r^2 - 2J_iJ_r\cos\Delta \tag{2.118}$$

To determine the inclination (A) and declination (B) of J we split J_i and J_r into their horizontal (J_{iH} and J_{rH}, respectively) and vertical components (J_{iV} and J_{rV}, respectively). Inclination is then derived as follows:

$$\begin{gathered} J_V = J_{iV} + J_{rV} \\ J_V = J_i \sin I + J_r \sin I_r \\ J \sin A = J_i \sin I + J_r \sin I_r \\ \sin A = \frac{J_i \sin I + J_r \sin I_r}{J} \\ A = \sin^{-1}\left(\frac{J_i \sin I + J_r \sin I_r}{J}\right) \end{gathered} \tag{2.119}$$

Similarly, declination it derived as follows:

$$\begin{gathered} J_H = J\cos A \\ J_H = J_{iH} + J_{rH} \\ J_H = J_i \cos I + J_r \cos I_r \\ J_H\hat{n} = J_H \cos B \\ J_H \cos B = J_{iH}\hat{n} + J_{rH}\hat{n} \\ J_H \cos B = J_{iH}\cos D + J_{rH}\cos D_r \\ J_H \cos B = J_i \cos I \cos D + J_r \cos I_r \cos D_r \\ \cos B = \frac{J_i \cos I \cos D + J_r \cos I_r \cos D_r}{J_H} \end{gathered}$$

$$B = cos^{-1}\left(\frac{J_i\, cos\, I\, cos\, D + J_r\, cos\, I_r\, cos\, D_r}{J\, cos\, A}\right) \tag{2.120}$$

The intensity of magnetization of magnetization in the x and z directions in the terms of total magnetization, J, in terms of A, B, C can be defined as:

$$J_x = J\cos(A)\cos(C - B) \tag{2.121}$$

$$J_z = J\sin(A) \tag{2.122}$$

The total intensity anomaly (T) can then be defined as:

$$T = V\sin(A) + H\cos(A)\cos(C - B) \tag{2.123}$$

2.6.2 Detailed derivation of Talwani and Heirtzler formulas to calculate magnetic anomalies caused by two dimensional structures of arbitrary shape

Rederiving equations (3) and (4) from Talwani and Heirtzler (1964), and equations (2.50) and (2.51) from our derivation for the vertical and horizontal components of the magnetic intensity. Talwani and Heirtzler (1964) begin their derivation not by defining x and z as shown in Figure 2.3, but defining x as:

$$x = x_1 + z_1 \cot(\phi) - z\cot(\phi) \tag{2.124}$$

$$x = x_2 + z_2 \cot(\phi) - z\cot(\phi) \tag{2.125}$$

gives

$$\cot(\phi) = \frac{x_1 - x_2}{z_2 - z_1} \tag{2.126}$$

This derivation fails as equation should be -cot(ϕ).

Using the equations for the Vertical and Horizontal Magnetic field and subbing in for x using Equation (2.124) we obtain

$$V = 2\int_{z_1}^{z_2} \frac{J_x z - J_z\left(x_1 + z_1 \cot(\phi) - z\cot(\phi)\right)}{\left(x_1 + z_1 \cot(\phi) - z\cot(\phi)\right)^2 + z^2} dz \tag{2.127}$$

$$H = 2\int_{z_1}^{z_2} \frac{J_x\left(x_1 + z_1 \cot(\phi) - z\cot(\phi)\right) + J_z z}{\left(x_1 + z_1 \cot(\phi) - z\cot(\phi)\right)^2 + z^2} dz \tag{2.128}$$

Rearranging gives

$$V = 2(J_x + J_z \cot(\phi)) \int_{z_1}^{z_2} \frac{z}{\left(x_1 + z_1 \cot(\phi) - zcot(\phi)\right)^2 + z^2} dz$$
$$-2J_z(x_1 + z_1 \cot(\phi)) \int_{z_1}^{z_2} \frac{dz}{\left(x_1 + z_1 \cot(\phi) - zcot(\phi)\right)^2 + z^2} dz \quad (2.129)$$

$$H = 2(J_z - J_x \cot(\phi)) \int_{z_1}^{z_2} \frac{z}{\left(x_1 + z_1 \cot\cot(\phi) - zcot(\phi)\right)^2 + z^2} dz$$
$$+2J_x(x_1 + z_1 \cot(\phi)) \int_{z_1}^{z_2} \frac{dz}{\left(x_1 + z_1 \cot(\phi) - zcot(\phi)\right)^2 + z^2} dz \quad (2.130)$$

Setting I_1 and I_2

$$I_1 = \int_{z_1}^{z_2} \frac{z}{\left(x_1 + z_1 \cot\cot(\phi) - zcot(\phi)\right)^2 + z^2} dz \quad (2.131)$$

$$I_2 = \int_{z_1}^{z_2} \frac{dz}{\left(x_1 + z_1 \cot\cot(\phi) - zcot(\phi)\right)^2 + z^2} \quad (2.132)$$

Solving the denominator

$$\left(x_1 + z_1 \cot(\phi) - zcot(\phi)\right)^2 + z^2$$

$$\left(1 + cot^2(\phi)\right)z^2 + \left(-2x_1 \cot(\phi) - 2z_1 cot^2(\phi)\right)z + (x_1 + z_1 \cot(\phi))^2 + cot^2(\phi))$$

$$A = \left(1 + cot^2(\phi)\right) \quad (2.132)$$

$$B = -2x_1 \cot(\phi) - 2z_1 cot^2(\phi) = 2\cot(\phi)\,(x_1 + z_1 co\,t(\phi)) \tag{2.133}$$

$$C = (x_1 + z_1 \cot(\phi))^2 + cot^2(\phi) \tag{2.134}$$

Equation I_1 becomes

$$I_1 = \int_{z_1}^{z_2} \frac{z}{Az^2 + Bz + C} dz \tag{2.135}$$

Equation I_2 becomes

$$I_2 = \int_{z_1}^{z_2} \frac{dz}{Az^2 + Bz + C} \tag{2.136}$$

Solving Equation I_1

$$I_1 = \frac{1}{2A} \int_{z_1}^{z_2} \frac{2Az + B}{Az^2 + Bz + C} dz - \frac{B}{2A} \int_{z_2}^{z_2} \frac{dz}{Az^2 + Bz + C} \tag{2.137}$$

$$I_1 = \frac{1}{2A} I_3 - \frac{B}{2A} I_2 \tag{2.138}$$

Solving I_3

$$I_3 = \int_{z_1}^{z_2} \frac{2Az + B}{Az^2 + Bz + C} dz \tag{2.139}$$

Substituting in

$$u = Az^2 + Bz + C \tag{2.140}$$

$$du = (2Az + B)dz \tag{2.141}$$

$$I_3 = \int \frac{1}{u} du \tag{2.142}$$

Solved as

$$I_3 = \ln|u| \tag{2.143}$$

Subbing back in for u

$$I_3 = \ln |\mathrm{A}z^2 + Bz + C| \Big|_{z_1}^{z_2}$$

$$I_3 = \ln|Az_2^2 + Bz_2 + C| - \ln|Az_1^2 + Bz_1 + C| \tag{2.144}$$

Solving $Az_1^2 + Bz_1 + C$

$$Az_1^2 + Bz_1 + C = \left(1 + \cot^2(\phi)\right)z_1^2 + \left(-2x_1\cot(\phi) - 2z_1\cot^2(\phi)\right)z_1 + (x_1 + z_1\cot(\phi))^2$$

$$Az_1^2 + Bz_1 + C = z_1^2\cot^2(\phi) - 2x_1z_1\cot(\phi) - 2\,z_1^2\cot^2(\phi)$$

$$Az_1^2 + Bz_1 + C = x_1^2 + 2x_1z_1 - 2z_1^2\cot^2(\phi)$$

$$Az_1^2 + Bz_1 + C = z_1^2 + x_1^2 = r_1^2 \tag{2.145}$$

Solving $Az_2^2 + Bz_2 + C$

$$\left(1 + \cot^2(\phi)\right)z_2^2 + \left(-2x_1\cot(\phi) - 2z_1\cot^2(\phi)\right)z_2 + (x_1 + z_1\cot(\phi))^2 \tag{2.146}$$

Rearranging

$$Az_2^2 + Bz_2 + C = \left(z_2^2 + z_2^2\cot^2(\phi)\right) = z_2^2 + x_2^2 \tag{2.147}$$

Plugging back into with $r_2^2 = z_2^2 + x_2^2$

$$I_3 = 2\ln\left|\frac{r_2}{r_1}\right| \tag{2.148}$$

Solving I_2, checking A is not equal to 0

$$A = 1 + cot^2(\phi) > 0 \tag{2.149}$$

Checking that $4AC - B^2 > 0$ for I_2

$$4\big(1 + cot^2(\phi)\big)(x_1 + z_1\cot(\phi))^2 - 4cot^2(\phi)(x_1 + z_1\cot(\phi))^2$$

$$\big(1 + cot^2(\phi) - cot^2(\phi)\big)(x_1 + z_1\cot(\phi))^2 = (x_1 + z_1\cot(\phi))^2 > 0 \tag{2.150}$$

Completing the square for the denominator

$$Az^2 + Bz + C = \sqrt{A}z + B + C - \frac{B^2}{A} \tag{2.151}$$

$$I_2 = \int_{z_1}^{z_2} \frac{dz}{\left(\sqrt{A}z + \frac{B}{2\sqrt{A}}\right)^2 + C - \frac{B^2}{4A}} \tag{2.152}$$

Applying substitution.

$$u = \sqrt{A}z + \frac{B}{2\sqrt{A}} \tag{2.153}$$

$$v^2 = C - \frac{B^2}{4A} \tag{2.154}$$

$$du = \sqrt{A}dz \tag{2.155}$$

Subbing in u and v gives

$$I_2 = \frac{1}{\sqrt{A}}\int \frac{du}{u^2 + v^2} \tag{2.156}$$

$$u = vtan(\beta) \tag{2.157}$$

$$du = vsec^2(\beta) + v^2 = v^2sec^2(\beta) \tag{2.158}$$

$$I_2 = \frac{1}{v\sqrt{A}}\int d\beta \tag{2.159}$$

$$I_2 = \frac{1}{\left(v\sqrt{A}\right)}(\beta_2 - \beta_1) \tag{2.160}$$

Checking β

$$\beta = tan^{-1}\left(\frac{u}{v}\right) \tag{2.161}$$

subbing back in u and v

$$\beta = tan^{-1}\left(\frac{\sqrt{A}z + \frac{B}{2\sqrt{A}}}{\sqrt{C - \frac{B^2}{A}}}\right) \tag{2.162}$$

Solving $z = z_1$ for the numerator equation (2.162)

$$2Az_1 + B = 2\left(1 + cot^2(\phi)\right)z_1 - 2x_1\cot(\phi) - 2z_1cot^2(\phi)1 - x_1\cot(\phi))$$

Solving $z = z_2$ for the numerator equation (2.162)

$$x_1 = x_2 + (z_2 - z_1)\cot(\phi)$$

$$2Az_2 + B = 2\left(1 + cot^2(\phi)\right)z_1 - 2x_1\cot(\phi) - 2z_1 cot^2(\phi)$$

$$2(2(z_2 - x_2\cot(\phi))$$

Solving the denominator for equation (2.162)

$$\sqrt{4AB - C^2} = \sqrt{4(x_1 + z_1\cot(\phi))^2}$$

$$\sqrt{4AB - C^2} = 2|x_1 + z_1\cot(\phi)|$$

Using $x_1 = x_2 + (z_2 - z_1)\cot(\phi)$

$$\sqrt{4AB - C^2} = 2|x_2 + z_2\cot(\phi)|$$

which gives,

$$\beta_1 = tan^{-1}\left(\frac{z_1 - x_1\cot(\phi)}{|x_1 + z_1\cot(\phi)|}\right) \quad (2.163)$$

$$\beta_2 = tan^{-1}\left(\frac{z_2 - x_2\cot(\phi)}{|x_2 + z_2\cot(\phi)|}\right) \quad (2.164)$$

Substituting back into V and H,

$$V = 2(J_x + J_z\cot(\phi))I_1 - 2J_z(x_1 + z_1\cot(\phi))I_2 \quad (2.165)$$

$$H = 2(J_z - J_x\cot(\phi))I_1 + 2J_x(x_1 + z_1\cot(\phi))I_2 \quad (2.166)$$

Subbing I_1 and I_2 back into V and H gives

$$V = 2(J_x + J_z\cot(\phi))\left(\frac{1}{2A}\ln\left|\frac{r_2}{r_1}\right| - \frac{B}{2A^{\frac{3}{2}}}(\beta_2 - \beta_1)\right) - \frac{2J_z(x_1 + z_1\cot(\phi))B}{2A^{\frac{3}{2}}}(\beta_2 - \beta_1) \quad (2.167)$$

$$H = 2(J_z - J_x \cot(\phi))\left(\frac{1}{2A}\ln\left|\frac{r_2}{r_1}\right| - \frac{B}{2A^{\frac{3}{2}}}(\beta_2 - \beta_1)\right) + \frac{2J_x(x_1 + z_1\cot(\phi))B}{2A^{\frac{3}{2}}}(\beta_2 - \beta_1) \quad (2.168)$$

Rearranging V and H and subbing in values for A, B, and C

$$V = 2\begin{pmatrix} J_x\left[sin^2(\phi)\ln\left|\frac{r_2}{r_1}\right| + \sin(\phi)\cos(\phi)\frac{x_1 + z_1\cot(\phi)}{|x_1 + z_1\cot(\phi)|}(\beta_2 - \beta_1)\right] \\ + J_z\left[-\sin(\phi)\cos(\phi)\ln\left|\frac{r_2}{r_1}\right| + sin^2(\phi)\frac{x_1 + z_1\cot(\phi)}{|x_1 + z_1\cot(\phi)|}(\beta_2 - \beta_1)\right] \end{pmatrix} \quad (2.169)$$

$$H = 2\begin{pmatrix} J_x\left[-\sin(\phi)\cos(\phi)\ln\left|\frac{r_2}{r_1}\right| + sin^2(\phi)\frac{x_1 + z_1\cot(\phi)}{|x_1 + z_1\cot(\phi)|}(\beta_2 - \beta_1)\right] \\ + J_z\left[sin^2(\phi)\ln\left|\frac{r_2}{r_1}\right| + \sin(\phi)\cos(\phi)\frac{x_1 + z_1\cot(\phi)}{|x_1 + z_1\cot(\phi)|}(\beta_2 - \beta_1)\right] \end{pmatrix} \quad (2.170)$$

Comparing to equations (3) and (4) in Talwani and Heirtzler (1964) we get the same answer with the exception of:

$$\delta = \frac{x_1 + z_1\cot(\phi)}{|x_1 + z_1\cot(\phi)|} \quad (2.171)$$

And θ from Talwani and Heirtzler (1964) $\neq \beta$ derived here.

Rewriting to get Q and P

$$P = -\sin(\phi)\cos(\phi)\ln\left|\frac{r_2}{r_1}\right| + sin^2(\phi)\frac{x_1 + z_1\cot(\phi)}{|x_1 + z_1\cot(\phi)|}(\beta_2 - \beta_1) \quad (2.172)$$

$$Q = sin^2(\phi)\ln\left|\frac{r_2}{r_1}\right| + \sin(\phi)\cos(\phi)\frac{x_1 + z_1\cot(\phi)}{|x_1 + z_1\cot(\phi)|}(\beta_2 - \beta_1) \quad (2.173)$$

using Talwani and Heirtzler definition of ϕ gives

$$P = \frac{z_{21}x_{12}}{z_{21}^2 + x_{12}^2} \ln\left|\frac{r_2}{r_1}\right| - \frac{z_{21}^2}{z_{21}^2 + x_{12}^2} \frac{x_1 + z_1 \cot(\phi)}{|x_1 + z_1 \cot(\phi)|} (\beta_2 - \beta_1) \tag{2.174}$$

$$Q = \frac{z_{21}^2}{z_{21}^2 + x_{12}^2} \ln\left|\frac{r_2}{r_1}\right| + \frac{z_{21}x_{12}}{z_{21}^2 + x_{12}^2} \frac{x_1 + z_1 \cot(\phi)}{|x_1 + z_1 \cot(\phi)|} (\beta_2 - \beta_1) \tag{2.175}$$

This shows dissimilarity with our derivation of the P and Q terms due to the different definition of the angle θ and the δ term in Talwani and Heirtzler (1964).

References

Jeshvaghani, M. S., Darijani, M. (2014). Two-dimensional geomagnetic forward modeling using adaptive finite element method and investigation of the topographic effect. *Journal of Applied Geophysics 105*, 169-179.

Talwani, M., Heirtzler, J. R., 1964. Computation of magnetic anomalies caused by two dimensional structures of arbitrary shape. *Computers in the mineral industries*, part 1: Stanford University publications, Geol. Sciences 9, 464-480.

Talwani, M., Heirtzler, J. R., 1962. The Mathematical Expression for the Magnetic Anomaly over a Two-Dimensional Body of Polygonal Cross Section. Lamont Doherty Geol. Obs. Columbia Univ., Tech. Rep. 6.

Talwani, M. (1965). Computation with the help of a digital computer of magnetic anomalies caused by bodies of arbitrary shape. *Geophysics 30*(5), 797-817.

Chapter 3: Paleogeography of the South China Block During the Ediacaran-Cambrian Transition

3.1. Introduction

The Ediacaran and its transition into the Cambrian represent one of the most significant and dynamic time periods in Earth's history. The beginning of the Ediacaran marked the end of the Marinoan glaciation (Knoll et al., 2006) the last of the Snowball Earth events of the Cryogenian (Hoffman and Schrag, 2002), and a transition to a favourable climate for multicellular organisms leading to the Cambrian explosion. Paleogeographically the final assemblage of Gondwana occurred between 650 – 500 Ma, which consisted of the amalgamation of Africa and South American terranes to Antarctica-Australia-India (Veevers, 2004).

Geochemically the precursor for the Cambrian explosion and oxygenation of the ocean is interpreted as negative ^{13}C isotope anomalies (Fike et al., 2006). The Shuram Wonoka excursion (SWE) is the largest negative carbon isotope anomaly in the Ediacaran with ^{13}C isotope values decreasing by greater than 15% reaching values of approximately -12% (Fike et al., 2006). The SWE is identified in four continents; Australia, Oman, South China, and Laurentia (Fike et al., 2006; Williams and Schmidt 2018 and references therein). The SWE is proposed to have lasted 10 Myr and stratigraphic correlations constrain the excursion to have occurred between 580 and 556 Ma (Williams and Schmidt, 2018; Gong et al., 2017). The SWE is still debated as having occurred during deposition or through diagenetic processes post deposition. For the SWE to occur during deposition this would require correlation between carbon and oxygen isotope

stratigraphic models that we do not see in present carbon cycles (Fike et al., 2006). If the SWE occurred due to diagenetic processes it would require a large-scale mechanism causing chemical modification of buried sediments of similar age such as tectonic uplift (Grotzinger et al., 2011). Fike et al. (2006) and McFadden et al. (2008) argued that the SWE is due to increased oxygenation of the world ocean from a large organic reservoir suspended in the deep ocean. Williams and Schmidt (2018) discussed that the SWE is a result of the world oceans causing the equator to become warmer than the poles causing an upwelling of anoxic ^{13}C depleted or oxygen enriched deep oceanic waters and constrained the SWE to have occurred within ±32° latitude of the equator. Adding further constraints to the paleogeography of the Earth at this time will give rise to better constrained models of climate and further understanding of the factors that allowed for the diversification and flourish of life.

The paleogeography of the South China Block (SCB) throughout the Ediacaran to the early Cambrian is highly debated and has led to the construction of many different and contradictory models for the location of the SCB (Qi et al., 2018; Li et al., 2018 and references therein). Interpretations of paleontological data summarized in Cocks and Torsvik (2013) and geochemical data in Qi et al. (2018) infer a close proximity of the SCB block to the western margin of Gondwana, however, interpretations of previous paleomagnetic studies for the Ediacaran of the SCB (Zhang and Piper, 1997; Macouin et al., 2004; Zhang et al., 2015; Gong et al., 2017) disagree with each other. Here we present new paleomagnetic data from Ediacaran aged rocks for the SCB that are from the well dated boundary of the Doushantuo and Denying formations at 551 Ma. Our new data resolve the problem of disagreement in the Ediacaran paleogeographic reconstructions of the SCB relatively to Gondwana.

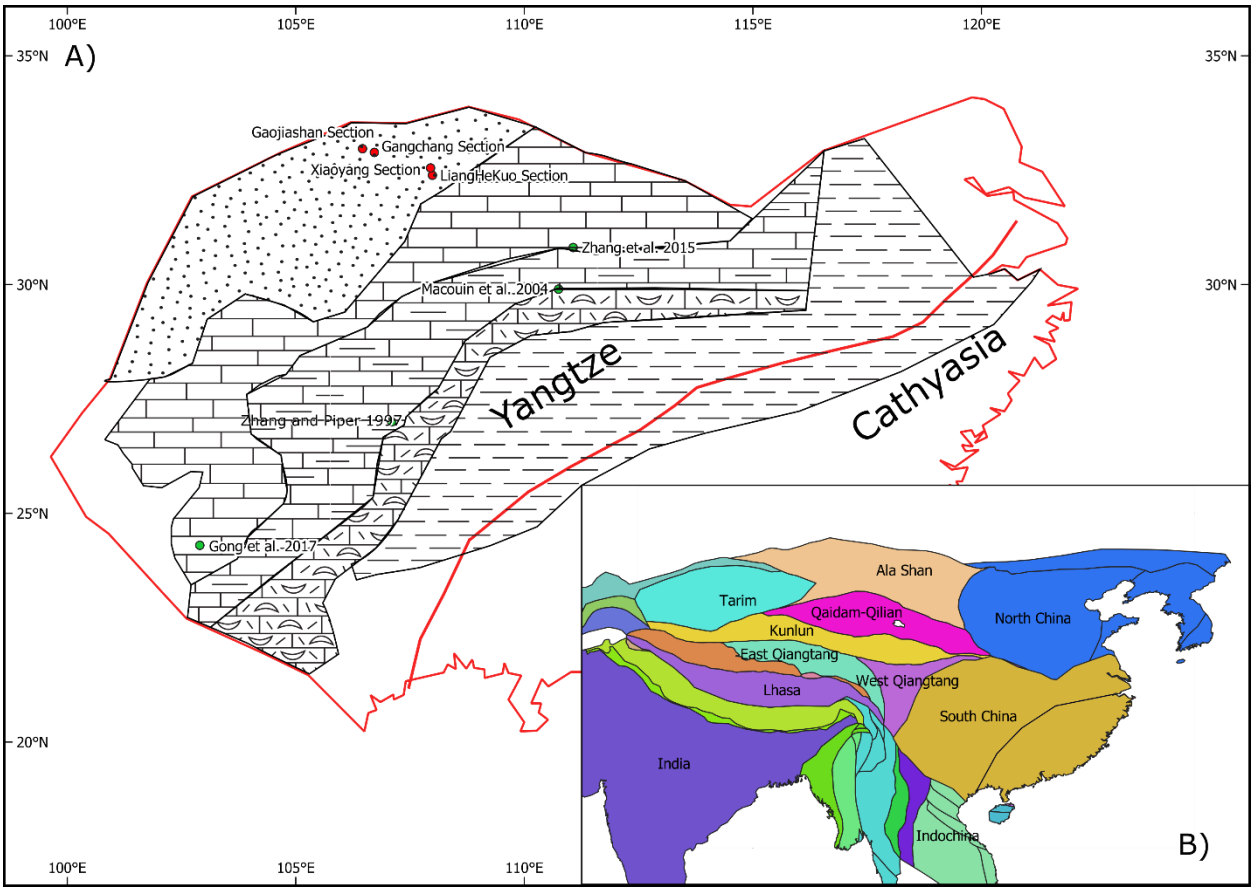

Figure. 3.1. Location of sampling sites with General tectonic setting and generalized Ediacaran geology. A) Location of sampled sections and major faults and folds with general geology of the SCB during the Ediacaran (modified from Jiang et al. (2011)). Red dots are our sampled sections green dots are the sampled sections of previous Ediacaran studies. The red outlines the SCB continental boundary with the Yangtze block to the north west and Cathyasia block to the south east. B) General tectonic framework of the Asian blocks modified from Mathews et al. (2016).

3.2. Geological background and sampling

The SCB is located in present day southeast China and is composed of two major Precambrian blocks; the Yangtze block in the northwest and the Cathaysia block in the southeast that amalgamated in the early to mid Neoproterozioc forming the Jiangnan orogen (Qi et al., 2018;

Cawood et al., 2018 and references therein). The SCB is bounded in the north to the North China Block by the Qinling-Dabie-Sulu orogen, in the east bounded to the Sogpan-Garze terran along the Longmentshan fault, and in the south to Indochina along the Ailaoshan-Song Ma suture zone (Cawood et al., 2018; Domeier, 2018).

The depositional environment throughout the Ediacaran on SCB has been interpreted as a shallow marine environment deposited along a passive margin with the depositional facies shallowing from the south east on the Cathaysia block to the north west on the Yangtze block (Jiang et al., 2011). The lithofacies are dominated by many transgressive and regressive sequences which has preserved many Ediacaran biota (Jiang et al., 2011).

Our paleomagnetic study was conducted in four sections on the north western margin of the SCB in the southern portion of the Shaanxi Province (Figure 3.1). The Gangchang (32.89° N, 106.72° E) and the GaoJiaShan (32.97° N, 106.46° E) sections, were brought to surface the folding and thrusting of the Longmen-Shen suture. The LiangHeKuo (32.39° N, 107.99° E), and Xiaoyang (32.55° N, 107.95° E) sections, were brought to surface by the East Qingling thrust system.

In our study locality the SCB for the Ediacaran formations are composed of the Doushantuo formation overlain by the Dengying formation. The age constraints on the Doushantuo formation are from two ash beds just above the cap dolostone of the Doushantuo formation (635 Ma) and an ash bed at the top of the Doushantuo formation (551.1) (Condon et al., 2005).

The Doushantuo formation in our study locations is exposed in the Gangchang, LiangHekou and Xiaoyang sections. In these sections the lithology of the Doushantuo formation consists of interbedded sandstones and siltstones, limestones, dolostones and mudstones. We have taken representative samples from each lithology with more sampling in the red sandstones and red mudstones as numerous studies have shown they provide favourable paleomagnetic results (Figure 3.2).

The Dengying formation was sampled in all four sections. In the Gaojiashan section of the SCB the Dengying formation is 621 m thick and is divided into three members, the Algal dolostone member, the Gaojiashan member (limestones and calcareous siltstones), and the Beiwan member (dolostones). These three members are correlated with the Hamajing, Shibantan and Baimatuo members in the Yangtze Gorges area of the SCB (Cui et al., 2019). In the Gangchang, LiangHeKuo, and Xiaoyang sections the Dengying formation is strictly the Algal dolomites.

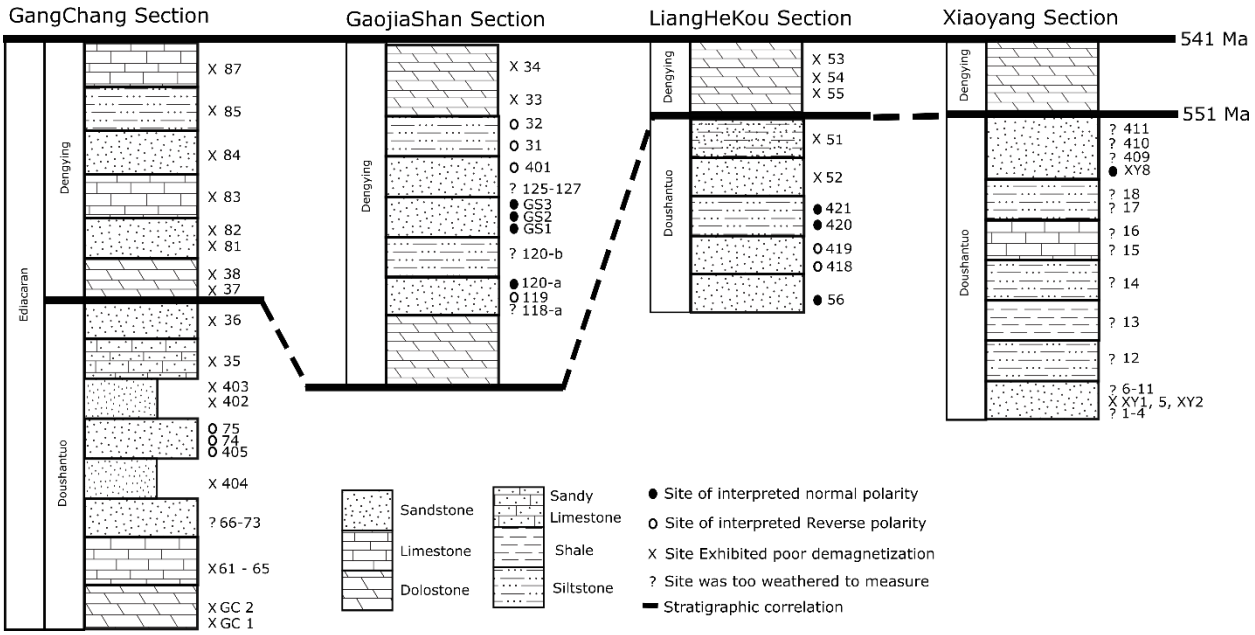

Figure. 3.2. Schematic stratigraphy of each sample site in each section and formation. The open circles are reverse polarity and the black circles are normal polarity sites, the X's indicate sites which exhibit poor magnetizations or absence of readable remnant magnetization, the ? are sites that were composed by the weathered rocks that produced unreliable results.

3.3. Methods

We took standard paleomagnetic drilling cores with a gasoline powered drill and oriented hand blocks. Hand blocks were taken in stratigraphic coordinates, registering the dip and azimuth of the dip, when the sediments were weathered and drilling was not possible. Cores and hand blocks were oriented in the field using a magnetic compass and a sun compass when weather permitted. There was no significant difference between the two measurements. The drilled cores were 2.2 cm in diameter and cut into samples with heights varying from 1 cm to 2.5 cm. The hand blocks were drilled and cut into cylindrical samples or were cut into cubic samples to a maximum size of 2.2x2.2x2.2 cm^3.

All measurements took place in three laboratories, 90% in the Laboratory of Paleomagnetism and Petromagnetism of the University of Alberta (Edmonton, Canada), and pilot samples were measured at the Ivar Giaever Geomagnetic Laboratory (University of Oslo, Norway) and Paleomagnetic Laboratory of the Northwest University (Xi'an, China). Measurements were performed with a 2G cryogenic magnetometer in all three labs and demagnetizations were carried out in the permalloy shielded room of the University of Alberta with ambient magnetic field less than 10 nT and MMLFC shielded room at the University of Oslo with ambient magnetic field 100 nT. Prior to measurements samples were stored in μ-metal shielded chamber or room. Thermal demagnetizations were carried out using the TD-48SC ASC thermal

demagnetizer and alternating field demagnetization was carried out using the 2G degaussing system. There was no systematic difference observed in results from the three laboratories.

Preliminary samples from each site were demagnetized at steps of 25 °C or 2 to 10 mT (AF) until the measurements became unstable or sporadic indicating mineralogical changes or spurious fields were acquired. The mineralogical changes were monitored by measurements of magnetic susceptibility after every temperature step for the pilot samples. Paleomagnetic directions are determined using principal component analysis (PCA) (Kirschvink, 1980) and constrained great circles (GC) fitting (McFadden and McElhinny, 1998). Paleomagnetic data was analyzed using the software packages PMGSC (Enkin, 1994) and PaleoMac (Congné. 2003).

To constrain the magnetic carrying minerals in our samples we performed temperature dependent magnetic susceptibility, IRM, and hysteresis measurements. Detailed rock magnetic measurements were performed on sites that represented primary magnetizations. Magnetic susceptibility measurements were carried out in an AGICO MFK1-FA Kappabridge with CS-4 furnace and processed with Cureval-8 software (Agico Inc). Hysteresis and IRM measurements were taken with a Lake Shore PMC MicroMag 3900 VSM.

3.4. Rock Magnetic Analysis

Rock magnetic studies were carried out only on sites in which demagnetizations were successful. We measured magnetic susceptibility versus temperature, IRM and hysteresis (Figure 3.3). The red sandstones (sites 74, 75, 405, 418, 419, 420) show a change in magnetic susceptibility above

600°C, are not saturated at high magnetic fields in IRM and have hysteresis indicative of hematite (Figure 3.3). The grey sandstones (sites 56, GS1, GS2) show a mixture of magnetite and hematite based on the wasp waisted shape of the hysteresis curves and not becoming saturated in high magnetic fields (Figure 3.3), with demagnetizations occurring by 600 °C or 680 °C. The siltstones (sites 31, 32, 421) are completely demagnetized by 600 °C which supports the presence of magnetite as the dominant carrier of the magnetic remanence. The Doushantuo and Dengying formations High temperature component (HTC) have been unblocked from 350 °C up to 680 °C with both directions and great circles (Figure 3.5). Due to the characteristic magnetization being carried by hematite the AF demagnetization did not completely demagnetize the samples and they were further treated by thermal demagnetization.

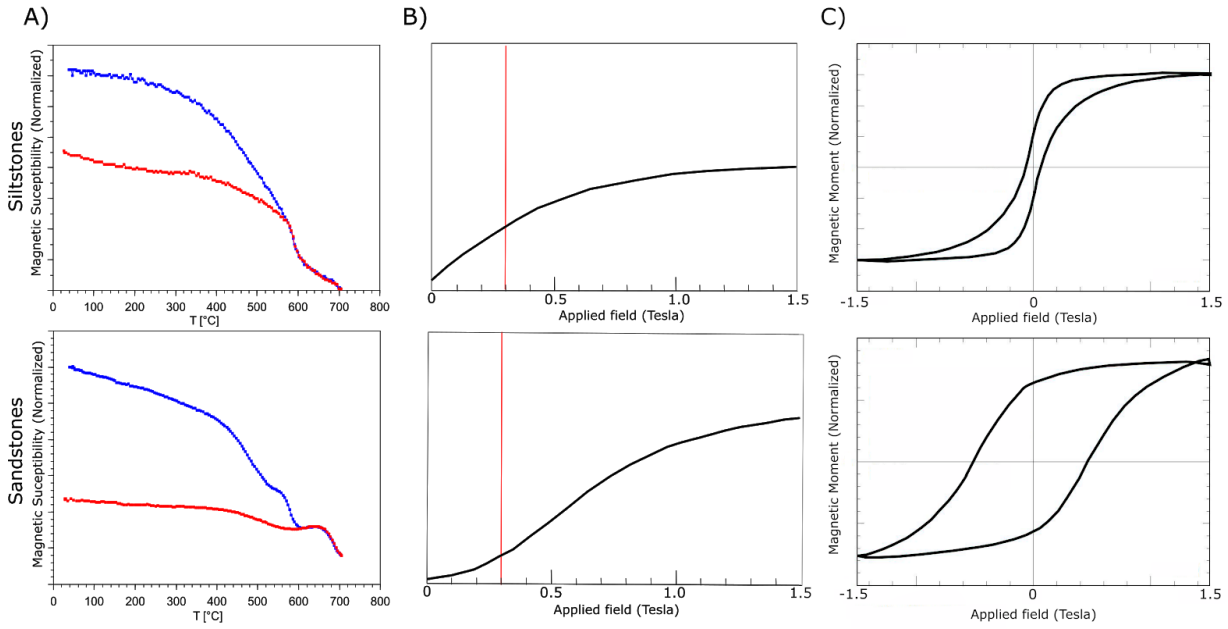

Figure. 3.3. A) Temperature vs relative magnetic susceptibility for representative samples of each lithology. B) IRM of representative samples the red line is 0.3T, C) relative hysteresis response.

3.5. Paleomagnetic analysis

3.5.1. Low temperature and low coercivity component

The NRM intensity of samples ranged from 1 to 10 mA/m. Low temperature or coercivity component (LC) is similar in all study locations and formations. LC is typically removed by 350 °C or 15 mT. Approximately 90% of LC are clearly be identified by principal component analysis Figure 3.4. LC clusters in situ (D_g = 9.1º, I_g = 53.3º, α_{95}=2.7º, k_g=25.9, n=110 samples) about a present day geomagnetic field direction in the study area calculated from IGRF https://www.geomag.nrcan.gc.ca/calc/mfcal-en.php (D_{PDF} = 3º, I_{PDF} = 51º) and scatters in tilt corrected system of coordinates (D_s = 29.9º, I_s = 19.0º, α_{95}=4.2º, k_s=11.5, n=110 samples) (Figure 3.4). We therefore interpret that LC is a Cenozoic or recent geomagnetic field overprint for the Ediacaran samples.

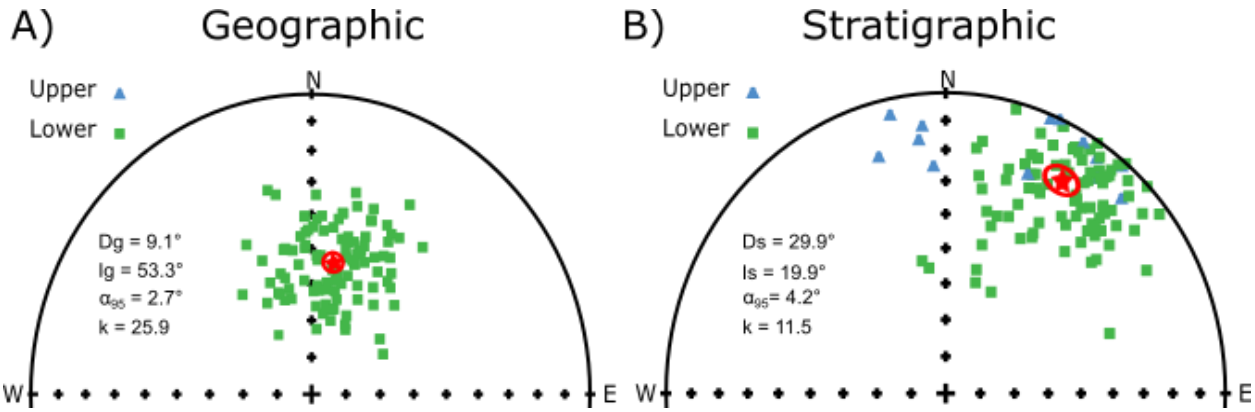

Figure. 3.4. LC sample level from all sections sampled. A) Geographic system of coordinates with the red star indicating the mean. B) geographic system of coordinates with the red star indicating the mean.

3.5.2. High Temperature Component (HTC)

3.5.2.1. Doushantuo formation (Ediacaran, 635-551.1 Ma)

The HTC is isolated above 450°C and has two polarities with the normal polarity preserved in the grey sandstones and blue siltstones and the reverse polarity in the red sandstone and siltstone beds. Both the normal polarity and reverse polarities are represented by great circles and PCA directions. The sites that preserve HTC are stratigraphically located at the top of the Doushantuo formation (Figure 3.2). The LiangHeKuo section shows two polarities with south west cluster for and north east cluster (Fig. 3.5, Table 3.1). The Xiaoyang section shows a north east cluster with a single polarity and the GangChang section only shows a single polarity clustering in the north west in stratigraphic coordinates.

Table 3.1. Ediacaran HTC site mean directions grouped into sections and formations. N is the number of specimens, Dec: declination; Inc: inclination, K: Fisher precision parameters; α_{95} is the 95% cone of confidence radius; All angles are in degrees. Bedding (strike/dip) are using the right-hand rule.

	Bedding			InSitu				Tilt Corrected			
Site ID	Strike	Dip	n	Dec	Inc	K	α_{95}	Dec	Inc	K	α_{95}
Doushantuo Formation											
Gang Chang Section											
75A	88	19	14	334.1	-1.1	4	22.7	333	16.2	4	22.7
75B	88	19	19	329.9	-23.2	10.1	11.1	332.5	16.2	10.1	11.1
405	80	9	7	307.1	2.5	38.1	9.9	306.5	9	38.1	9.9
LiangHeKuo Section											
56	334	64.3	16	180.8	-50	16.6	10.5	209.2	-5.6	15.4	10.1
418	338	62	12	360	27.6	10.3	14.2	12.3	-3.8	10.2	14.3
419	334	67	11	339.8	36.4	46	6.8	9.8	9.7	46	6.8
420	337	60	14	180.6	-26.6	42.1	6.2	191.7	4.9	42.1	6.2
421	325	68	8	177.1	-58	21.7	12.9	208.3	-3.2	21.7	12.9
Xiaoyang Section											
XY2	329	44.4	7	345.1	4.8	21.5	13.3	348.6	13.4	15.9	15
XY8	345.5	49.7	10	31.7	58.8	31.8	8.7	53.7	15.5	31.8	8.7
Dengying Formation											
Gaojiashan Section											
31	261	64	7	83.3	71.3	16.7	15.2	11.3	25.4	16.7	15.2
32	260.6	64	8	47.5	67.1	15.9	14.3	10.6	15	15.9	14.3
GS1	253	57.5	8	242.6	-51	6.3	24	203.9	-18.8	6.3	24
GS2	253	57.5	9	234.1	-43.6	10.8	17	207.1	-10	10.8	16.9
120	258	58	10	7	59.1	36.5	8.1	358	2.5	36.5	8.1

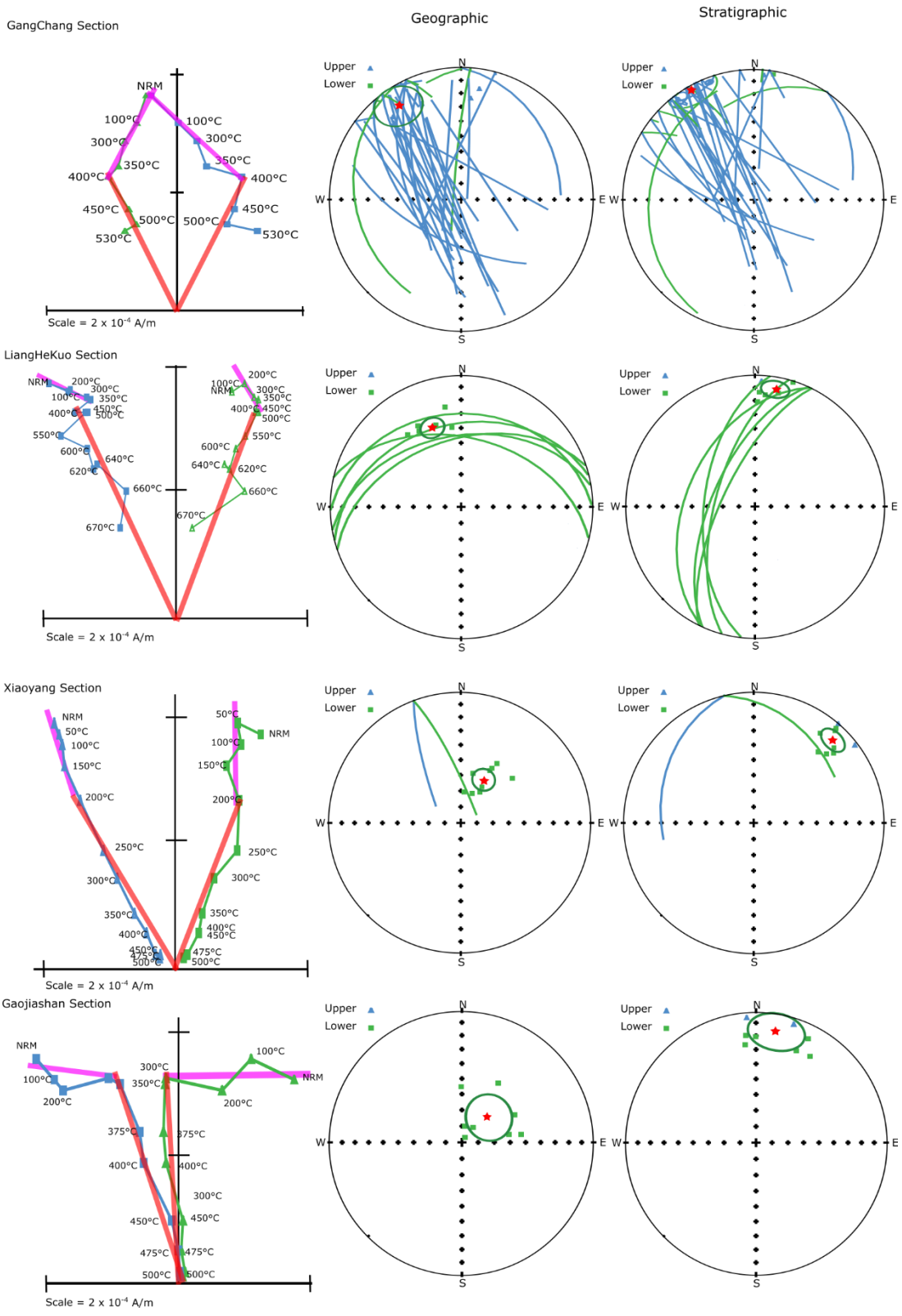

Figure 3.5. Results of thermal demagnetization for the Ediacaran. The Doushantuo formation is represented in the Gangchang, LiangHeKuo, and Xiaoyang sections. Samples from the Dengying

formation is represented in the Gaojiashan section. The purple lines represent the LC the red lines on the Zijderveld diagram represent the HTC. The red star indicates the site mean. Typical orthogonal vector plots during thermal demagnetization are in-situ coordinates. Square (triangle) symbols in orthogonal plots: projections onto the horizontal (vertical) plane; temperature steps are indicated in degrees Celsius. Equal-area projections of site-mean directions of HTC, with circles of 95% confidence.

3.5.2.2. Dengying formation (551.1 – 541 Ma)

The Dengying formation was sampled in all four sections but HC have only been found in the Gaojiashan section which has different lithology (grey sandstones, silstones) than the other sampled sections (dolostones). The HTC component has been isolated above 350°C been preserved in the grey sandstones siltstones, and red mudstones clustering in the south west and north east with both PCA and GC analysis (Fig. 3.5, Table 3.1).

3.5.2.3. Ediacaran directions

Lithologically it was found that the red sandstones carried a negative polarity and the blue siltstones and grey sandstones carried a normal polarity. The entirety of sites from the Xiaoyang section show no discernible difference between the HTC's and LC's and in geographic coordinates clustered about the present-day field which we interpret the entire section was likely remagnetized in the Cenozoic and will be subject to no further analysis. The Gangchang section is separated from the Gaojiashan section by a strike slip fault indicating rotation as well as the HTC's only showing single polarity, we separate it for interpretation. The Gaojiashan and LiangHekuo sections are both exposed due to thrusting from different aged events and show

similarities in HTC directions as well as stratigraphically close positions are combined for further analysis.

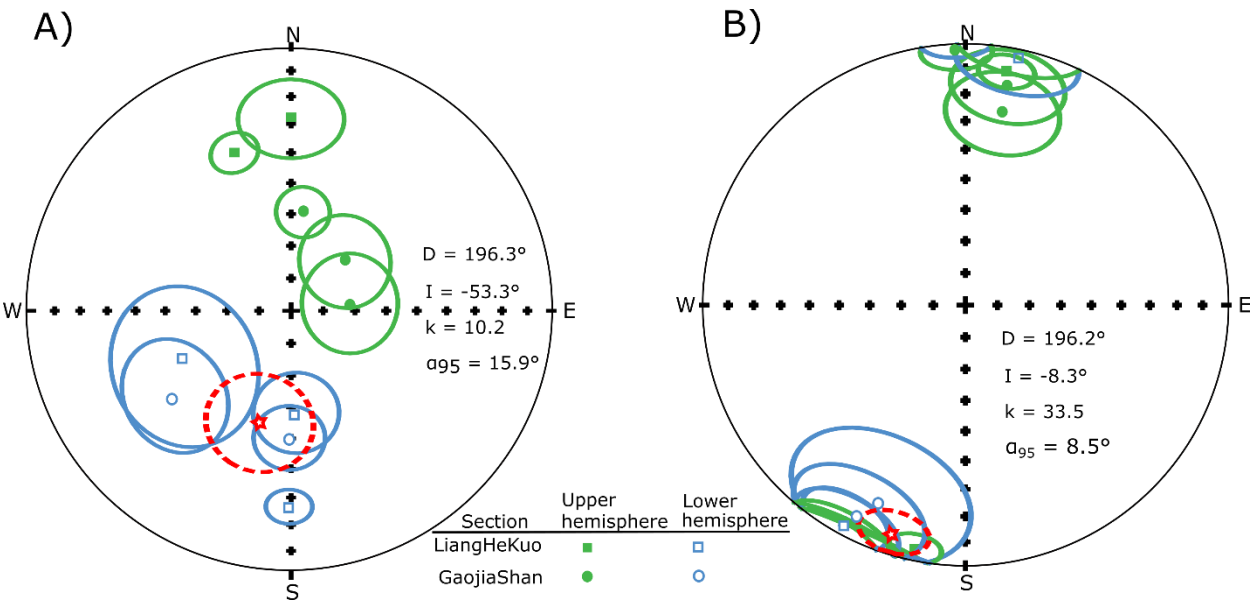

Figure 3.6. Site means of the Ediacaran formations. A) is in geographic coordinate system and B) is in Stratigraphic coordinate system. The infilled green shapes are in the upper hemisphere and the open blue shapes are in the lower hemisphere. The red star is the mean direction of all the sites.

The HTC's from the Gaojiashan and LiangHeKuo sections are presented in Table 3.1. We calculate the site average direction for the 10 sites from the two sections and obtain a mean direction in geographic coordinates (D_g = 196.3°, I_g = –53.3°, k_g = 10.2, α_{95} = 15.9°) and in stratigraphic coordinates (D_s = 196.2°, I_s = –8.3°, k_s = 33.5, α_{95} = 8.5°). The direction in stratigraphic coordinates passes the McElhinny (1964) fold test above 95% (k_s/k_g = 3.27, n=10 sites). The McFadden (1990) fold test is positive at the 99% level ($Xi1_g$ = 3.297 and $Xi1_s$ = 0.3596; $Xi2_g$ = 8.095 and $Xi2_s$ = 1.237; critical $Xi_{95\%}$ = 3.685 and $Xi_{99\%}$ = 5.120). The reversal test of McFadden and McElhinny (1990) is positive in class C with a critical gamma of 17.0° at

95% confidence, the angle between the two polarity mean directions = 10.4°, critical R at 95% = 0.171, F(2*(n2-1),2*(n1-1) at point 5% = 4.060).

Inclination shallowing has been proposed to affect many paleomagnetic studies on sedimentary rocks and is dependant on many factors such as matrix grain size, magnetic mineral, compaction, and sedimentation rates, thus is different for every study. To quantify the impacts of inclination shallowing on our samples we apply the method of inclination elongation to our HTC's as proposed by Tauxe and Kent (2004). Our results on the 68 samples that provided us directions, which is much less than the recommended 100 samples recommended, and 1000 bootstrap resampling was an average flattening factor of 0.4. Appling this inclination shallowing factor to our site mean increases the inclination to –20.0°, which would indicate that our samples experienced significant shallowing (Figure 3.7). It is worth noting that this is a blanket calculation (applying a single correction to all samples), and due to our less than optimal sample size varying lithologies and magnetic carrying minerals for the elongation inclination technique that a singular flattening factor is not appropriate to apply to our study.

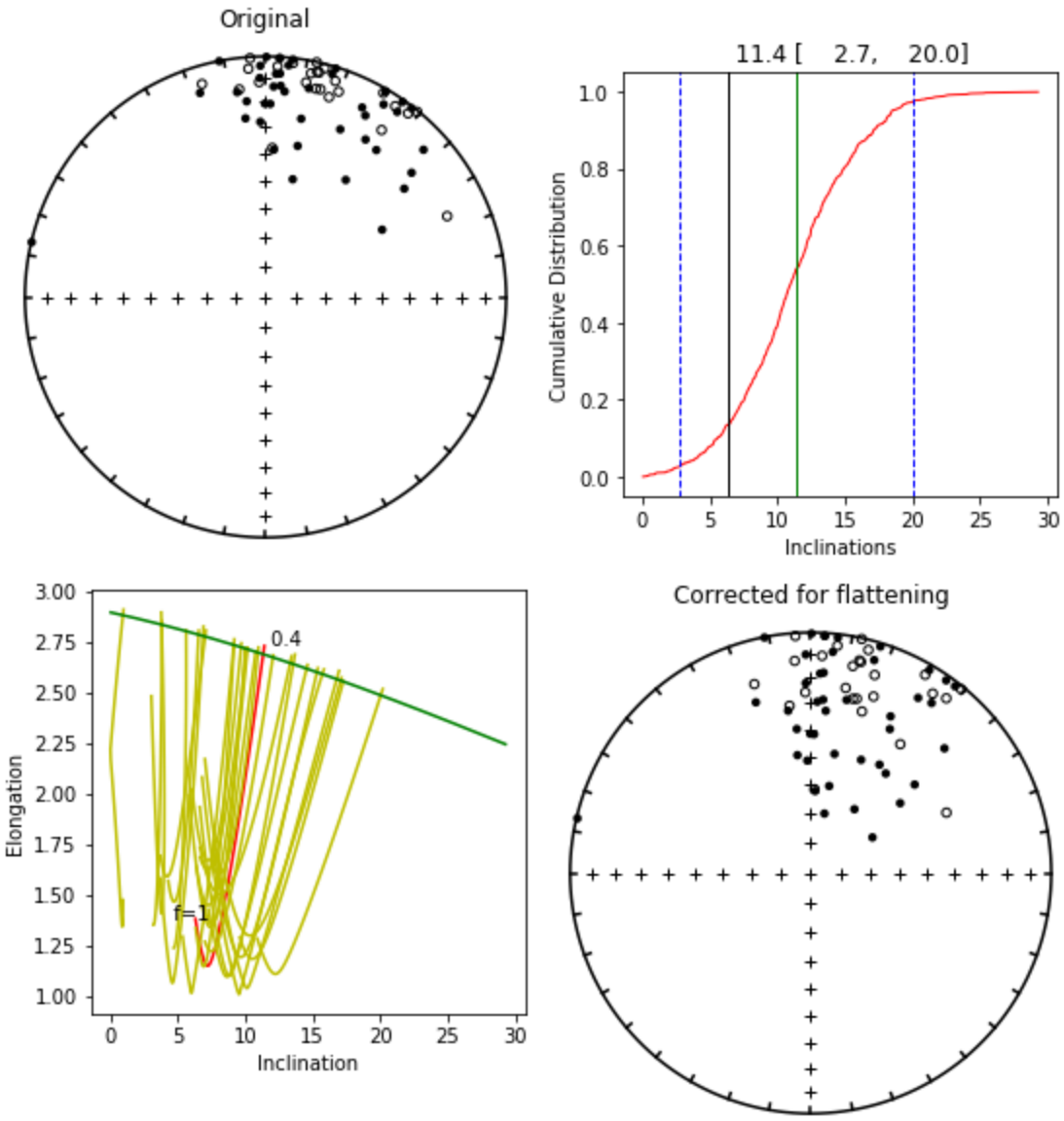

Figure 3.7. Application of the Elongation Inclination technique from Tauxe and Kent (2004). The test was run with a total number of 1000 bootstraps from a total number of directions of 68. The result is an inclination shallowing factor of 0.4. The confidence bounds are 2.7° to 20.0° with a mean of 11.4°.

Positive fold and reversal tests, absence of metamorphism in and near the sampling locality, magnetite and hematite as primary minerals that carry remnant enable us to assume that the average direction of the HTC is most likely primary magnetization for the Gaojiashan and

LiangHeKuo sections. A new paleomagnetic pole was calculated for the tilt-corrected system of coordinates 57.9 °S and 75.0 °E (dm = 8.6°, dp = 4.3°) with a paleolatitude of 4.2 °S ± 4.3° (Figure 3.8 pole 1). This new pole does not resemble any younger paleomagnetic pole.

From the Gangchang section we get a section mean of D_g = 145.4°, I_g = 9.1°, k_g = 22.7, α_{95} = 19.7° in geographic coordinates and D_s = 146.1°, I_s = –5.5°, k_s = 25.6, α_{95} = 18.5°. There is not a large dip for the Gangchang section which explains why the geographic and stratigraphic coordinates are similar. Using the stratigraphic coordinate system, we produce a paleomagnetic pole of 46.4 °S and 160.6 °E (dp = 18.6°, dm = 9.3°) with a paleolatitude of 2.8 °S ± 9.3° (Figure 3.8 Pole 2). This pole only has one polarity, and no fold test but it does not resemble any younger paleopoles in either geographic or stratigraphic systems of coordinates (Figure 3.8 pole 2).

3.6. Discussion

3.6.1. Comparison of paleomagnetic poles

We obtain two poles for the Ediacaran. Pole 1 is sampled from the LiangHeKuo and Gaojiashan sections and pole 2 is from the Gangchang section. Pole 1 has a quality factor of 7 based on Van der Voo (1990) criteria, this includes positive fold and reversal tests, no resemblance to younger poles, adequate demagnetization with PCA, the age is well dated within 20 Ma (551 Ma), and sufficient samples with a confidence cone less than 16°. We interpret pole 1 as the primary magnetization and present the first reliable Ediacaran pole for the SCB. Pole 2 only has one polarity and has no fold test. We plot the two poles in Figure 3.8. We find that the rotation angle

between these two poles from pole 1 to pole 2 is 52.17° CCW. This could possibly be due to tectonic rotation or a remagnetization of the HTC of the Gangchang section. Pole 1 differs notably from previous studies (Zhang et al., 2015; Macouin et al., 2004, Gong et al., 2017) (Figure 3.8, Table 3.2).

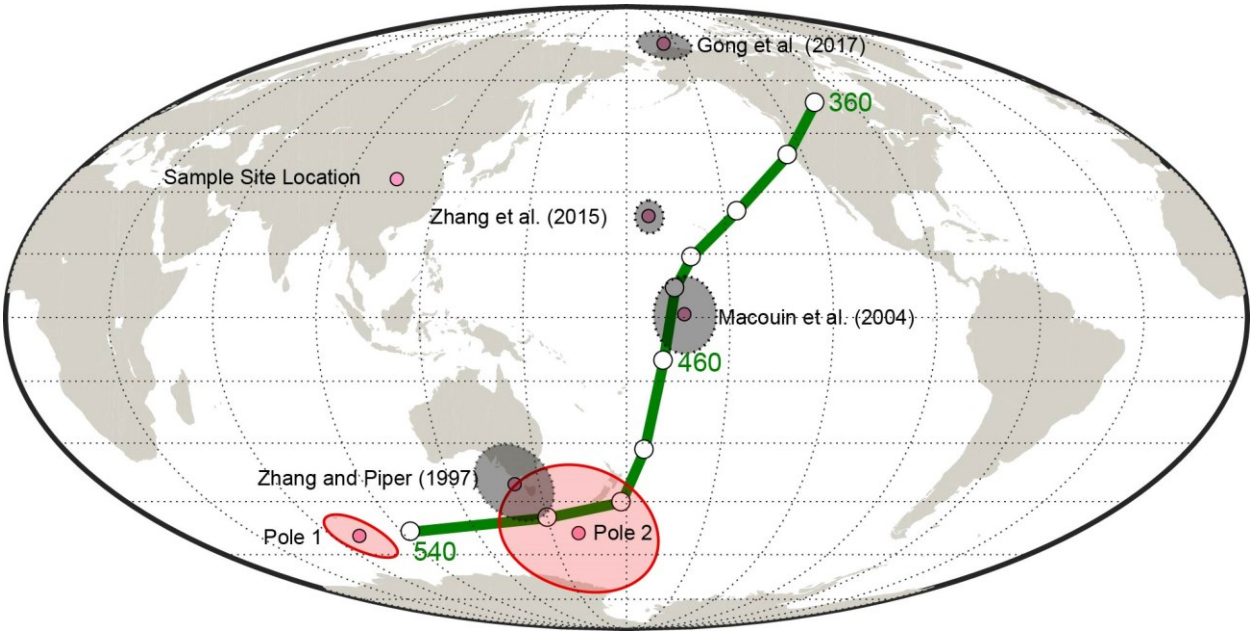

Figure 3.8. Ediacaran paleomagnetic poles and newly constructed Middle – Early Paleozoic segment of APWP for the SCB. Pole 1 refers to the pole calculated from the Gaojiashan, and LiangHeKuo. Pole 2 refers to the pole calculated from the Gangchang section. See Table 3.2 for poles used for APWP and ages of Ediacaran poles. The figure is plotted using PMTec2015 software from Wu et al. (2015). The APWP is constructed using splines with the smoothing parameter of 300 and an interpolation of 20 Ma.

There have been four previous studies of Ediacaran rocks from the SCB (Zhang et al., 2015; Macouin et al., 2004; Gong et al., 2017). Zhang et al. (2015) study locality was in the Jiulongwan section where they took samples from member 3 of the Doushantuo formation (600-584 Ma). Zhang et al. (2015) pole has two polarities but fails to properly constrain a fold test due

to the shallow dipping nature of the fold limbs sampled. Zhang et al. (2015) pole resembles the Triassic portion of the APWP. Macouin et al. (2004) study was from member 3 of the Doushantuo formation (600-584 Ma) in the Shiman section of the Hunan province that was folded in the Jurassic. They present positive fold tests though they report only a single polarity. Their pole strongly resembles the Silurian pole of the SCB (Table 3.2). Gong et al. (2017) reported the Dongdahe section Member three and suggested a possibility of Mesozoic remagnetization due to the late Mesozoic Yanshanian orogeny in the Cretaceous due to its single polarity and resemblance to the Cenozoic paleomagnetic poles. Zhang and Piper (1997) proposed three poles from rocks at the top of the Nantuo formation dated at the end of the Cryogenian and the bottom of the Doushantuo formation, dated at the beginning of the Ediacaran from Wong'an, South China. Their Ediacaran pole provides only a single polarity, has no fold test and resembles close to more recently published Cambrian poles and pole 2 from the Gangchang section.

We conclude that other poles published for Ediacaran rocks do not meet the full criteria to be considered primary magnetization due to lack of reliability tests and similarities to younger paleomagnetic poles, these poles should not be used for constructing the APWP or plate tectonic reconstructions. In order to create a new APWP for the SCB we use the compilation of middle to early Paleozoic poles from Domeier (2018), with the addition of our new Ediacaran pole 1 (Table 3.2). To calculate the APWP we use the PMtech 2015 software (Wu et al., 2015) using a spherical spline with a smoothing parameter of 300 and an interpolation of 20 Ma (Figure 3.8).

Table 3.2. Paleomagnetic poles for the SCB and APWP. Age is age in Ma, Plong is paleolongitude, Plat is Paleolatitude. Paleomagnetic poles of the SCB from 385 Ma are on the left with the APWP on the right. APWP is generated using a spherical spline and a smoothing parameter of 300.

Paleomagnetic Poles					APWP		
Age	Plong	Plat	Used in APWP	Study	Age	Plat	Plong
385	236.4	33.6	Yes	Xian et al., 2019	360	51	252
432	196.1	14.9	Yes	Huang et al., 2000	380	40	235
432	194.7	4.9	Yes	Opdyke et al., 1987	400	28	219
456	191.3	-45.8	Yes	Han et al., 2015	420	16	202
470	154.9	-38.4	Yes	Hanning et al., 1998	440	2	194
503	185.1	-39.5	Yes	Lixin et al., 1998	460	-25	190
503	166	-51.3	Yes	Yang et al., 2004	480	-42	184
551	75	-57.9	Yes	This Study Pole 1	500	-46	178
551	161	-53.9	No	This Study Pole 2	520	-55	151
595	187	23.9	No	Zhang et al 2015	540	-58	93
590	203	71.8	No	Gong et al. (2015)			
600	197	0.6	No	Macouin et al. (2004)			
630	141.8	-40.6	No	Zhang and Piper (1997)			

3.7. Paleogeographic Reconstruction

The difficult debate as to the location of the SCB and its relationship to India and Australia is coming closer to a consensus. Interpretations of paleontological data place the SCB to the western margin of Gondwana (Cocks and Torsvik, 2013; Domeier, 2018) and references therein). Qi et al. (2018) suggest that detrital zircons are derived from the India block throughout the Ediacaran and infer that the SCB was in close proximity of India throughout the Ediacaran. With our new well dated and reliable paleomagnetic pole we have paleolatitude and orientation constraint on the SCB at the end of the Ediacaran. We can confidently place the SCB off the northern portion of India as an integral part of Gondwana (Figure 3.9). The southern edge of the SCB in the present-day coordinates was facing north.

Figure 3.9. 550 Ma paleogeographic reconstruction of the SCB relative to Torsvik and Cocks, (2013) Gondwana based on our new pole 1 for the SCB. Only the major blocks that compose Gondwana are shown. Figure was created using the Gplates software (Muller et al., 2018). The red contour corresponds to the continental shelf of Gondwana. Comparing to Figure 1.1 the reconstructions for the SCB have been significantly improved.

3.8. Conclusions

Our study provides the first reliable paleomagnetic pole for the South China Block for the late Ediacaran. The reliability of this pole is solidified by well constrained age, α_{95} less than 16°, PCA of directions, absence of significant metamorphism, passing the fold and reversal tests, and lack of resemblance to any younger paleomagnetic poles, passing all seven criteria outlined in Van der Voo (1990). Pole 1 differs significantly from previously published Ediacaran. Due to the depositional environment indicating a passive margin (Jiang et al., 2011), sedimentary source rocks for the SCB derived from India (Qi et al., 2018), combined with our paleomagnetic results we place the SCB off the northern portion of India and west of Australia as part of east Gondwana at the end of the Ediacaran. The present day south of the SCB faces north in the Ediacaran reconstruction.

The new paleogeographic reconstruction for the SCB indicates that it was a significant member of Gondwana to which three of the four continents that have the formations that the Shuram Wonoka excursion (SWE) is found. With the final amalgamation of Gondwana occurring after the deposition of the formations that host the SWE, this could indicate that the SWE occurred during final amalgamation of Gondwana. As the proximity of Laurentia to Gondwana is still debated that hypothesis may not be resolved.

Chapter 4: Conclusions

In conclusion this thesis has crucial implications on modelling magnetic anomalies (Chapter 2) and Ediacaran paleogeography (Chapter 3). First by providing the corrected algorithm for fast modelling of irregular 2-dimensional bodies along with computational software which is available at the website www.ualberta.ca/~vadim/software.htm and second by providing the first reliable paleomagnetic pole for the SCB at the Ediacaran Cambrian transition.

Upon close inspection of the derivation of equations originally published by Talwani and Heirtzler (1964), erroneous definitions were used leading to incorrect solutions for forward modeling of particular 2D geometries; this is outlined in chapter 2. These errors if made by themselves produce large discrepancies in the forward modelling of the magnetic field but if all made together then can produce the correct answer. It is unclear when these errors will cause instabilities and incorrect anomalies. We present a new algorithm and transparency in derivation, that has been proofed several times and produces stable answers to which we recommend that it be used for future modelling and for verification of old models. For user friendly implementation of this algorithm we created a Matlab GUI and executable for those who do not have Matlab. Features of our software include; calculation of remnant magnetization direction if the paleomagnetic pole is known, single calculation using both induced and remnant magnetizations, importing of data from processing software's in either profile of gridded data, and exporting models. To further the software for academic use additions of error analysis and interactions of model fitting to determine a best fit curve can be obtained using least squares polynomial fits.

We provide a new paleomagnetic pole for the Ediacaran of the SCB that passes all reliability tests for primary magnetization, which is the first from the SCB. With our new Ediacaran paleomagnetic pole we are finally able to construct the APWP for the SCB into the Ediacaran. We are also able to produce the first constrained paleogeographic reconstruction for the SCB at the Ediacaran Cambrian boundary. In this new construction we place the SCB along the eastern margin of Gondwana connected to India. This new reconstruction allows to constraint future modelling of climate, environment and geochemical events prior to the Cambrian explosion. To further understand the final amalgamation of Gondwana throughout the Ediacaran the next step would be to combine the Neoproterozoic paleomagnetic poles of the SCB and India and compare them to the APWP of the rest of the Gondwana continents to determine the final assemblage of the supercontinent.

The next largest of the Asian blocks after the SCB is the North China Block (NCB), also lacks paleomagnetic data in the Ediacaran which has led to a significant number of unconstrained models (Figure 1.1, Figure 3.9) (Li et al., 2018; Mckenzie et al., 2011; Cocks and Torsvik, 2013). Cambrian trilobite similarity has led to the consensus that the North China Block was in some proximity of the SCB though that is the only constraint on its location in the Ediacaran (Mckenzie et al., 2011), therefore paleomagnetic study is necessary to constrain the position of the NCB. A paleomagnetic study of the NCB will require much the same style of sampling and approach as was taken in our study of the SCB as there has been no previous paleomagnetic studies on Ediacaran rocks. This will require new field work and systematic measurements of each lithology to determine if there is primary remnant magnetization present.

References

Cawood, P. A., Zhao, G., Yao, J., Wang, W., Xu, Y., & Wang, Y. (2018). Reconstructing South China in phanerozoic and precambrian supercontinents. *Earth-Science Reviews*, *186*, 173-194.

Charvet, J. (2013). The Neoproterozoic–early Paleozoic tectonic evolution of the South China Block: an overview. *Journal of Asian Earth Sciences*, *74*, 198-209.

Cocks, L. R. M., & Torsvik, T. H. (2013). The dynamic evolution of the Palaeozoic geography of eastern Asia. *Earth-Science Reviews*, *117*, 40-79.

Cogné, J.P., 2003. PaleoMac: a Macintosh™ application for treating paleomagnetic data and making plate reconstructions. *Geochemistry, Geophysics, Geosystems*, 4(1).

Condon, D., Zhu, M., Bowring, S., Wang, W., Yang, A., & Jin, Y. (2005). U-Pb ages from the neoproterozoic Doushantuo Formation, China. *Science*, *308*(5718), 95-98.

Cui, H., Xiao, S., Cai, Y., Peek, S., Plummer, R. E., & Kaufman, A. J. (2019). Sedimentology and chemostratigraphy of the terminal Ediacaran Dengying Formation at the Gaojiashan section, South China. *Geological Magazine*, 1-25.

Driscoll, P. E., & Evans, D. A. (2016). Frequency of Proterozoic geomagnetic superchrons. *Earth and Planetary Science Letters*, *437*, 9-14.

Domeier, M. (2018). Early Paleozoic tectonics of Asia: Towards a full-plate model. In *Geoscience Frontiers* (Vol. 9, Issue 3, pp. 789–862).

Enkin, R.J., 1994. A computer program package for analysis and presentation of paleomagnetic data. *Pacific Geoscience Centre, Geological Survey of Canada*, 16.

Fike, D. A., Grotzinger, J. P., Pratt, L. M., & Summons, R. E. (2006). Oxidation of the Ediacaran ocean. *nature*,*444*(7120), 744.

Gong, Z., Kodama, K. P., & Li, Y. X. (2017). Rock magnetic cyclostratigraphy of the Doushantuo Formation, South China and its implications for the duration of the Shuram carbon isotope excursion. *Precambrian Research*, *289*, 62-74.

Grotzinger, J. P., Fike, D. A., & Fischer, W. W. (2011). Enigmatic origin of the largest-known carbon isotope excursion in Earth's history. *Nature Geoscience*, *4*(5), 285.

Hoffman, P. F., & Schrag, D. P. (2002). The snowball Earth hypothesis: testing the limits of global change. *Terra nova*, *14*(3), 129-155.

Jeshvaghani, M. S., & Darijani, M. (2014). Two-dimensional geomagnetic forward modeling using adaptive finite element method and investigation of the topographic effect. Journal of Applied Geophysics, 105, 169-179.

Jiang, G., Shi, X., Zhang, S., Wang, Y., & Xiao, S. (2011). Stratigraphy and paleogeography of the Ediacaran Doushantuo Formation (ca. 635–551 Ma) in south China. *Gondwana Research*, *19*(4), 831-849.

Jiao, W., Li, Y. X., Yang, Z., & Liu, J. (2019). A Widespread Early Mesozoic Remagnetization in South China. *Journal of Geophysical Research: Solid Earth*, *124*(1), 88-103.

Kostrov, N. P. (2007). Calculation of magnetic anomalies caused by 2D bodies of arbitrary shape with consideration of demagnetization. Geophysical prospecting, 55(1), 91-115.

Lelievre, P.G., & Oldenburg, D.W. (2006). Magnetic forward modelling and inversion for high susceptibility. Geophysical Journal International, 166 (1), 76-90.

Li, S., Zhao, S., Liu, X., Cao, H., Yu, S., Li, X., ... & Suo, Y. (2018). Closure of the Proto-Tethys Ocean and Early Paleozoic amalgamation of microcontinental blocks in East Asia. *Earth-Science Reviews*, *186*, 37-75.

Kirschvink, J. L. (1980). The least-squares line and plane and the analysis of palaeomagnetic data. *Geophysical Journal International*, *62*(3), 699-718.

Macouin, M., Besse, J., Ader, M., Gilder, S., Yang, Z., Sun, Z., & Agrinier, P. (2004). Combined paleomagnetic and isotopic data from the Doushantuo carbonates, South China: implications for the "snowball Earth" hypothesis. *Earth and Planetary Science Letters*, *224*(3-4), 387-398.

Matthews, K. J., Maloney, K. T., Zahirovic, S., Williams, S. E., Seton, M., & Mueller, R. D. (2016). Global plate boundary evolution and kinematics since the late Paleozoic. *Global and Planetary Change*, *146*, 226-250.

McElhinny, M. W., & McFadden, P. L. (1998). *The magnetic field of the earth: paleomagnetism, the core, and the deep mantle* (Vol. 63). Academic Press.

McFadden, K. A., Huang, J., Chu, X., Jiang, G., Kaufman, A. J., Zhou, C., ... & Xiao, S. (2008). Pulsed oxidation and biological evolution in the Ediacaran Doushantuo Formation. *Proceedings of the National Academy of Sciences*, *105*(9), 3197-3202.

McKenzie, N. R., Hughes, N. C., Myrow, P. M., Choi, D. K., & Park, T. Y. (2011). Trilobites and zircons link north China with the eastern Himalaya during the Cambrian. *Geology*, *39*(6), 591-594.

Müller, R. D., Cannon, J., Qin, X., Watson, R. J., Gurnis, M., Williams, S., ... & Zahirovic, S. (2018). GPlates: Building a virtual Earth through deep time. *Geochemistry, Geophysics, Geosystems*, *19*(7), 2243-2261.

Olson, P., Landeau, M., Reynolds, E., True dipole wander, *Geophysical Journal International*, Volume 215, Issue 3, 1 December 2018, Pages 1523–1529, https://doi.org/10.1093/gji/ggy349

Qi, L., Xu, Y., Cawood, P. A., & Du, Y. (2018). Reconstructing Cryogenian to Ediacaran successions and paleogeography of the South China Block. *Precambrian Research*, *314*, 452-467.

Raub, T. D., Kirschvink, J. L., & Evans, D. A. D. (2007). True polar wander: linking deep and shallow geodynamics to hydro-and bio-spheric hypotheses. *Treatise on geophysics*, *5*, 565-589.

Talwani, M., & Heirtzler, J. R., 1962. The Mathematical Expression for the Magnetic Anomaly over a Two-Dimensional Body of Polygonal Cross Section. Lamont Doherty Geol. Obs. Columbia Univ., Tech. Rep. 6.

Talwani, M., Heirtzler, J. R., 1964. Computation of magnetic anomalies caused by two dimensional structures of arbitrary shape. *Computers in the mineral industries*, part 1: Stanford University publications, Geol. Sciences, 9, 464-480.

Talwani, M. (1965). Computation with the help of a digital computer of magnetic anomalies caused by bodies of arbitrary shape. Geophysics, 30(5), 797-817.

Tauxe, L., & Kent, D. V. (2004). A simplified statistical model for the geomagnetic field and the detection of shallow bias in paleomagnetic inclinations: was the ancient magnetic field dipolar?.

Torsvik, T. H., & Cocks, L. R. M. (2013). Gondwana from top to base in space and time. *Gondwana Research*, *24*(3-4), 999-1030.

Torsvik, T. H., & Cocks, L. R. M. (2017). *Earth History and Palaeogeography*.

Torsvik, T. H., van der Voo, R., Doubrovine, P. V., Burke, K., Steinberger, B., Ashwal, L. D., ... & Bull, A. L. (2014). Deep mantle structure as a reference frame for movements in and on the Earth. *Proceedings of the National Academy of Sciences*, *111*(24), 8735-8740.

Van der Voo, R. (1990). The reliability of paleomagnetic data. *Tectonophysics*, *184*(1), 1-9.

Veevers, J. J. (2004). Gondwanaland from 650–500 Ma assembly through 320 Ma merger in Pangea to 185–100 Ma breakup: supercontinental tectonics via stratigraphy and radiometric dating. *Earth-Science Reviews*, *68*(1-2), 1-132.

Williams, G. E., & Schmidt, P. W. (2018). Shuram–Wonoka carbon isotope excursion: Ediacaran revolution in the world ocean's meridional overturning circulation. *Geoscience Frontiers*, *9*(2), 391-402.

Won, I. J., & Bevis, M. (1987). Computing the gravitational and magnetic anomalies due to a polygon: Algorithms and Fortran subroutines. Geophysics, 52(2), 232-238.

Wu, L., Kravchinsky, V. A., & Potter, D. K. (2015). PMTec: A new MATLAB toolbox for absolute plate motion reconstructions from paleomagnetism. *Computers & geosciences*, *82*, 139-151.

Zhang, S., Li, H., Jiang, G., Evans, D. A., Dong, J., Wu, H., ... & Xiao, Q. (2015). New paleomagnetic results from the Ediacaran Doushantuo Formation in South China and their paleogeographic implications. *Precambrian Research*, *259*, 130-142.

Zhang, Q. R., & Piper, J. D. A. (1997). Palaeomagnetic study of Neoproterozoic glacial rocks of the Yangzi Block: palaeolatitude and configuration of South China in the late Proterozoic Supercontinent. *Precambrian Research*, *85*(3-4), 173-199.